Current Research in Neurobiology 5 (2023) 100112

Contents lists available at ScienceDirect

Current Research in Neurobiology

journal homepage: www.sciencedirect.com/journal/current-research-in-neurobiology

The SARS-CoV-2 spike glycoprotein interacts with MAO-B and impairs mitochondrial energetics

Chantal A. Pileggi [a,b,c], Gaganvir Parmar [a,b], Hussein Elkhatib [a,b], Corina M. Stewart [a,b,d], Irina Alecu [a,b,e], Marceline Côté [a,b,f], Steffany A.L. Bennett [a,b,e], Jagdeep K. Sandhu [a,b,f,g], Miroslava Cuperlovic-Culf [a,b,c,1], Mary-Ellen Harper [a,b,f,*,1]

[a] Department of Biochemistry, Microbiology and Immunology, Faculty of Medicine, University of Ottawa, 451 Smyth Road, Ottawa, ON, K1H 8M5, Canada
[b] Ottawa Institute of Systems Biology, University of Ottawa, ON, K1H 8M5, Canada
[c] National Research Council of Canada, Digital Technologies Research Centre, 1200 Montreal Road, Ottawa, ON, K1A 0R6, Canada
[d] Current Address: Faculty of Medicine, University of British Columbia, Vancouver, BC, Canada
[e] Neural Regeneration Laboratory, Department of Biochemistry, Microbiology and Immunology, Faculty of Medicine, University of Ottawa, 451 Smyth Road, Ottawa, ON, K1H 8M5, Canada
[f] Centre for Infection, Immunity and Inflammation, University of Ottawa, ON, K1H 8M5, Canada
[g] Human Health Therapeutics Research Centre, National Research Council Canada, 1200 Montreal Road, Ottawa, ON, K1A 0R6, Canada

ARTICLE INFO

Keywords:
SARS-CoV-2
Monoamine oxidase B
Mitochondria
Parkinson's disease

ABSTRACT

SARS-CoV-2 infection is associated with both acute and post-acute neurological symptoms. Emerging evidence suggests that SARS-CoV-2 can alter mitochondrial metabolism, suggesting that changes in brain metabolism may contribute to the development of acute and post-acute neurological complications. Monoamine oxidase B (MAO-B) is a flavoenzyme located on the outer mitochondrial membrane that catalyzes the oxidative deamination of monoamine neurotransmitters. Computational analyses have revealed high similarity between the SARS-CoV-2 spike glycoprotein receptor binding domain on the ACE2 receptor and MAO-B, leading to the hypothesis that SARS-CoV-2 spike glycoprotein may alter neurotransmitter metabolism by interacting with MAO-B. Our results empirically establish that the SARS-CoV-2 spike glycoprotein interacts with MAO-B, leading to increased MAO-B activity in SH-SY5Y neuron-like cells. Common to neurodegenerative disease pathophysiological mechanisms, we also demonstrate that the spike glycoprotein impairs mitochondrial bioenergetics, induces oxidative stress, and perturbs the degradation of depolarized aberrant mitochondria through mitophagy. Our findings also demonstrate that SH-SY5Y neuron-like cells expressing the SARS-CoV-2 spike protein were more susceptible to MPTP-induced necrosis, likely necroptosis. Together, these results reveal novel mechanisms that may contribute to SARS-CoV-2-induced neurodegeneration.

1. Introduction

Severe acute respiratory syndrome coronavirus 2 (Mitochondrial metabolic manipulation by SARS-CoV-2 in peripheral blood mononuclear cells of patients with COVID-19), which causes COVID-19 disease, primarily infects the respiratory tract and acutely manifests with pneumonia-like symptoms (Zhu et al., 2020, pp. 727–733). Neurological symptoms are common and reported in up to 70–80% of COVID-19 hospitalized patients (Helms et al., 2020; Mao et al., 2020); however, SARS-CoV-2 symptoms typically resolve soon after recovery from the initial infection. Some patients report persistent neurocognitive symptoms associated with continued post-COVID myalgic encephalomyelitis/chronic fatigue syndrome as part of "long-COVID" symptoms (Stefano et al., 2021; Taquet et al., 2021). Although substantial brain invasion is uncommon, the neurotropism of SARS-CoV-2 has been established as SARS-CoV-2 antigens and RNA have been detected in neurons, microglia, and astrocytes in brain tissue from deceased COVID patients (Crunfli et al., 2022; Matschke et al., 2020; Song et al., 2021;

* Corresponding author. Department of Biochemistry, Microbiology and Immunology, Faculty of Medicine, University of Ottawa, 451 Smyth Road, Ottawa, ON, K1H 8M5, Canada.
E-mail address: mharper@uottawa.ca (M.-E. Harper).
[1] Co-senior authors.

https://doi.org/10.1016/j.crneur.2023.100112
Received 14 March 2023; Received in revised form 21 August 2023; Accepted 25 September 2023
Available online 6 October 2023

Stein et al., 2022). Resulting cerebral infections are associated with a broad array of acute and chronic pathological changes, including cerebrovascular damage, the presence of acute/sub-acute infarcts, hypometabolism, reduced global brain size, and decreased grey matter thickness (Douaud et al., 2022; Guedj et al., 2021; Hosp et al., 2021; Manca et al., 2021; Mukerji and Solomon, 2021; Raman et al., 2021). Neuroinflammation and neurodegeneration can occur independently of SARS-CoV-2 neuroinvasion, highlighting the molecular complexity associated with acute and persistent neurocognitive symptoms (Fernández-Castañeda et al., 2022).

The SARS-CoV-2 spike (S) protein is responsible for facilitating viral entry by mediating fusion between the virus and host cell membranes. The S protein is a class I viral fusion glycoprotein consisting of the S1 subunit which contains the receptor binding domain, the S2 subunit which harbors the fusion peptide (Ou et al., 2020). For viral entry to occur, the S protein needs to be primed and activated to transition from a high-energy metastable state to a low-energy state (Harrison, 2015; Ou et al., 2020). Priming and activation of the S protein occurs through proteolytic processing and binding to the host cell receptor, angiotensin-converting enzyme 2 (ACE2) (Hoffmann et al., 2020; Ou et al., 2020; Shang et al., 2020a). Endothelial cells that line the blood-brain barrier (BBB) and epithelial cells of the choroid plexus express ACE2 and are thought to facilitate entry of SARS-CoV-2 into the central nervous system (CNS) (Krasemann et al., 2022; Pellegrini et al., 2020). The S1 subunit can readily cross the BBB and widespread entry of S1 into the brain may also contribute to the development of neurocognitive symptoms (Rhea et al., 2021). Olfactory neurons in the olfactory epithelium have relatively low ACE2 expression, but SARS-CoV-2 entry into the CNS may be facilitated by neuropilin-1 and/or transmission from non-neuronal olfactory cells that have high ACE2 expression (Butowt and Bilinska, 2020; Cantuti-Castelvetri et al., 2020).

There is mounting evidence that SARS-CoV-2 targets mitochondria and manipulates metabolism with mitochondrial dysfunction mirroring that seen in neurodegenerative disease (Ajaz et al., 2021; Gibellini et al., 2020; Ramachandran et al., 2022). Infection with SARS-CoV-2 is associated with changes in mitochondrial morphology, altered bioenergetic function, increased reactive oxygen species (ROS), and decreased mitochondrial membrane potential (Ajaz et al., 2021; Romão et al., 2022; Shang et al., 2021). Moreover, the S protein can interact with endogenous proteins and modulate cellular processes in the absence of the other SARS-CoV-2 viral components (Shirato and Kizaki, 2021; Solis et al., 2022; Suzuki et al., 2021), including mitochondrial function and the NLRP3 inflammasome (Albornoz et al., 2022; Clough et al., 2021; Lei et al., 2021). These changes led us to ask whether SARS-CoV-2 spike glycoprotein might enhance apoptosis or necroptosis in response to environmental toxins associated with neurodegenerative disease.

Our group has recently shown that the substrate binding region of monoamine oxidase B (MAO-B) has 95–100% structural homology with the ACE2 receptor binding region (Cuperlovic-Culf et al., 2021). MAO-B is an outer mitochondrial membrane flavoprotein that is highly expressed in the substantia nigra and periventricular nucleus and catalyzes the oxidative deamination of biogenic amines, including dopamine and 2-phenylethylamine (Obata et al., 2022). Oxidation of MAO-B substrates stoichiometrically results in H_2O_2 production, implicating MAO-B in cell death and mitochondrial dysfunction (Nagatsu and Sawada, 2006; Tipton, 2018). Age-related increases in MAO-B expression are also associated with neurodegeneration through increases in ROS production that can perturb mitochondrial function, leading to the loss of dopaminergic neuron viability (Mallajosyula et al., 2008). Hence, MAO-B inhibitors are frequently employed as a therapeutic intervention in Parkinson's disease to attenuate neurodegeneration (Dezsi and Vecsei, 2017). Computational modelling suggests that the interaction between the S protein and MAO-B may alter neurotransmitter metabolism by affecting access of neurotransmitters to the active binding site of MAO-B, or by modifying the electrostatic environment (Cuperlovic-Culf et al., 2021; Hok et al., 2022). Patients with COVID-19 disease have high platelet MAO-B gene expression (Manne et al., 2020), suggesting that dysregulated monoamine metabolism may be a consequence of SARS-CoV-2 infection. Likewise, MAO-B was the top upregulated gene in transcriptomic profiling of whole blood from patients with severe > moderate > mild COVID-19 disease (Broderick et al., 2022). Emerging evidence suggests that SARS-CoV-2 may be linked to post-encephalitic Parkinsonism, as SARS-CoV-2 infection has recently been shown to sensitize dopaminergic neurons in the substantia nigra to mitochondrial stress-induced cell death in mice expressing the human ACE2 receptor (Smeyne et al., 2022). Understanding the neurological sequelae of SARS-CoV-2 is of particular importance when considering the surge of post-encephalitic Parkinsonism that followed the Spanish influenza in 1918 (Cunha, 2004).

Given the established role of MAO-B in Parkinson's disease and the potential interaction between the SARS-CoV-2 S protein and MAO-B, our primary aim was to establish if the S protein and MAO-B interact and alter MAO-B activity, thereby sensitizing SH-SY5Y neuron-like cells to PD-like neurodegeneration. Here, we demonstrate that the SARS-CoV-2 S protein interacts with cellular MAO-B *in vitro* and augments MAO-B activity. Furthermore, we show that S protein perturbs mitophagy, leading to the accumulation of aberrant mitochondria and increased sensitivity to 1-methyl-4-phenyl-1,2,3,6- tetrahydropyridine (MPTP)-induced necrosis.

2. Methods

2.1. HEK293T transient overexpression

Human Embryonic Kidney (HEK) 293 T cells were cultured in Dulbecco's modified Eagles' Medium (DMEM; Gibco) supplemented with 10% heat-inactivated FBS (Wisent Bio Products) and 1% antibiotic/antimycotic solution (Gibco) and were maintained at 37 °C with 5% CO_2. Upon 70% confluency, HEK293T cells were transiently transfected with 3 μg of plasmid using Lipofectamine LTX with Plus Reagent according to the manufacturer's protocol (Thermo Fisher Scientific, 15,338,100). Cells were harvested 48 h post-transfection for downstream experiments.

For the PLA assay, HEK293T cells were transfected with 3 μg of either control plasmid (pcDNA3.1+), a N-terminal FLAG-tagged SARS-CoV-2 spike (pCMV14-3X-FLAG-SARS-CoV-2 S, Addgene #145780), and/or a C-terminal HA-tagged MAO-B (pCMV6-MAO-B-HA). The HA-tagged MAO-B expression plasmid was constructed through *Xho*I/*Fse*I restriction digestion of pCMV6-MAO-B-FLAG plasmid (Origene #RC205320) to remove the FLAG-tag cDNA, followed by re-ligation via HiFi DNA Assembly (New England Biolabs) using a spacer sequence encoding an in-frame HA-tag.

For the co-immunoprecipitation assays, HEK293T cells were transfected with 3 μg of either a control plasmid (pcDNA3.1+), a C-terminal C9-tagged SARS-CoV-2 spike plasmid (pcDNA3.1+ SARS-Spike-C9, Addgene #145031 (Shang et al., 2020b)) and/or a C-terminal FLAG-tagged MAO-B expression plasmid (pCMV6-MAO-B-FLAG) (Origene #RC205320, Rockville, MD).

2.2. SH-SY5Y cell culture

Human SH-SY5Y neuroblastoma cells were cultured in a 1:1 mixture of Ham's F12 Nutrient Mixture (Gibco) and DMEM supplemented with 10% heat-inactivated FBS (heat-inactivated, Wisent) and 1% antibiotic/anti-mycotic solution (Gibco). To differentiate SH-SY5Y cells, the 1:1 mixture of Ham's F12 Nutrient Mixture and DMEM cell media was supplemented with 1% heat-inactivated FBS, 1% antibiotic/anti-mycotic solution, and 10 μM all-*trans*-retinoic acid (Sigma-Aldrich) for 7 days, with medium replaced every 2–3 days.

2.3. Generation of SH-SY5Y cells that stably express SARS-CoV2-spike-HA or empty vector

A stable SH-SY5Y cell line expressing a C-terminal HA-tagged SARS-CoV2-Spike glycoprotein was generated via lentiviral transduction of pBOB-CAG SARS-CoV2-Spike-HA lentiviral particles (Addgene #141347-LV). Cells were then selected using 300 μg/ml of Zeocin (InvivoGen, San Diego, CA). Successful selection was confirmed by immunoblotting and immunocytochemistry with HA-tag antibody (Cell Signaling, #3724).

An empty lentiviral backbone was constructed from the pBOB-CAG SARS-CoV2-Spike-HA plasmid (Addgene #141347) through *ClaI/Xho*I restriction digestion to remove the spike glycoprotein cDNA, followed by re-ligation via HiFi DNA Assembly (New England Biolabs) using a spacer sequence. Packaging plasmids pCMV-VSVG and pCMV-Gag-Pol (Cell biolabs, inc.), and the empty vector backbone construct were co-transfected into unmodified HEK293T cells using Lipofectamine LTX reagent (ThermoFisher) in a 1:2:3 ratio. Fourty-eight hours post transfection, viral supernatant was harvested and filtered through a 0.45 μm filter. One mL of viral supernatant was combined with 400,000 SH-SY5Y cells and 8 μg/ml hexadimethrine bromide and centrifuged at 800 g for 1 h. Cells were then incubated with viral supernatant for 48 h, followed by replacement media supplemented with 300 μg/ml of Zeocin (InvivoGen, San Diego, CA).

2.4. Immunofluorescence, proximity ligation assays, and microscopy

For immunofluorescence experiments, all cells seeded onto 12 mm coverslips coated with Matrigel (Corning) were fixed with 4% paraformaldehyde for 15 min. Fixed cells were washed three times with PBS and subsequently permeabilized in blocking buffer (PBS containing 1% BSA and 0.5% Triton X-100) containing the primary antibodies for 1.5 h [1° antibodies: Rhodopsin C9 (Millipore, MAB5356; 1:200), anti-FLAG M2 (Sigma, F1804; 1:200), anti-HA (Cell Signaling, 3724, 1:200), and/or mtHSP70 [JG1] (ThermoFisher, MA3-028, 1:100), LAMP1 (ProteinTech, 21997, 1:200)]. Coverslips were washed with 1x PBS and then incubated with anti-rabbit or anti-mouse fluorescent secondary antibodies diluted in 1x PBS containing 10 μg/ml Hoechst counter-stain (Invitrogen) for 2 h [2° antibodies anti-Mouse IgG (H + L) Alexa Fluor 568 (Invitrogen, A-11004, 1:200) and anti-rabbit IgG (H + L) Cy5 (Jackson ImmunoResearch, 711-175-152,1:200). Coverslips were washed again and mounted using Shandon™ Immu-Mount solution (Fisher Scientific). Immunofluorescence images were captured using a Zeiss LSM880 AxioObserver Z1 confocal microscope with AiryScan using a 63×, 1.4 NA oil objective. Images were processed using ZenBlue 3.2 software (Zeiss). Mitochondrial area per cell was performed by quantifying the area of mtHSP70 using ImageJ software and normalising to the number of nuclei per image (manual count). Colocalization between LAMP1 and mtHSP70 was determined semi-automatedly using ImageJ by analysing the colocalized area fraction (% overlap) and with the JACOP plug-in to determine the Mander's correlation coefficient (Bolte and Cordelières, 2006).

PLA assays were performed according to the manufacturer's protocol (Sigma, DUO92008). In brief, HEK293 cells were permeabilized with 0.5% Triton X-100, and blocked in the provided buffer for 30 min. HA (Cell Signaling, 3724, 1:200) and FLAG primary antibodies (Sigma, F1804; 1:200) were incubated on the samples for 1 h, followed by incubation with appropriate secondary antibodies, ligation and amplification solutions, according to the manufacturer's protocol.

2.5. Co-immunoprecipitation

HEK293T cells were transiently transfected as described above, with 3 μg of either control plasmid (pcDNA3.1+), SARS-CoV-2-Spike-C9 and/or a MAO-B-FLAG expression plasmids. Fourty-eight hours following transient transfection, cells were lifted with trypsin, washed by resuspension in PBS, and pellets were stored at −80 °C until further use. Pellets were resuspended in 1x lysis buffer (50 mM Tris HCl, 150 mM NaCl, 1 mM EDTA, 1% Triton X-100, pH 7.4) supplemented with a protease cocktail inhibitor (Sigma Aldrich; P8340). Cells were lysed by passing through a 31-gauge needle and subsequently centrifuged at 14,000 g for 10 min. The supernatant was collected and passed through a 45 μm filter. Protein concentration of the filtrate was determined using the Bradford method, and an aliquot was stored for the analysis of the whole cell lysate sample. The remaining filtrate was then incubated on a rotating platform with anti-FLAG M2 magnetic beads (Sigma A2220) overnight at 4 °C. The following day, the tubes were placed on a magnetic rack, and the supernatant was removed. The remaining protein complexed to the M2 beads was washed twice in TBS, and protein was eluted by gently mixing with 50 μL of buffer containing 0.1 M glycine HCL (pH 3.0). Ten μL of neutralization buffer (0.5 M Tris, 1.5 M NaCl, pH-8.0) was then added to the eluted protein. Samples were prepared for SDS-PAGE in Laemmli buffer and boiled for at 95 °C for 5 min. Analysis by immunoblotting was performed by probing with either anti-C9 tag (anti-Rhodopsin C9, Millipore MAB5356) or anti-FLAG M2 (Sigma F1804).

2.6. MAO-B radiometric activity assay

MAO-B radiometric activity assays were performed in triplicate for both cell homogenates and enriched mitochondrial fractions. Mitochondrial isolations were performed as previously described (Spinazzi et al., 2012). MAO activity was monitored using ^{14}C-labeled phenylethylamine as previously described (Tipton et al., 2000). Briefly, 75 μg of total protein or 25 μg of enriched mitochondria were incubated with 20 μM ^{14}C-labeled phenylethylamine in a 100 mM potassium phosphate buffer (pH 7.4) at 37 °C for 30 min. The reaction was terminated by the addition of 100 μl 2 M citric acid solution and the ^{14}C-labeled phenylethylamine was extracted with ethyl acetate/toluene (1:1) and centrifuged at 5000 *g* at 4 °C for 10 min. The organic phase containing the reaction product was extracted and transferred into liquid scintillation cocktail (Ultima Gold™ MV, PerkinElmer), and counted on a Tri-Carb 4910 TR Beta Liquid Scintillation Analyzer (PerkinElmer). Specific activity is expressed in pmol/min/mg protein.

2.7. H_2O_2 emissions

Two million cells resuspended in Buffer Z (in mM: 110 K-MES, 35 kC l, 1 EGTA, 3 $MgCl_2$, 5 K_2HPO_4, and 0.5 mg/ml BSA; pH 7.3, 37 °C) and incubated with 1.5 U ml^{-1} horseradish peroxidase, 1.5 μM of Amplex red, and digitonin (4.05 μM) at 37 °C. For mitochondrial H_2O_2 emissions, baseline fluorescence readings were taken prior to the addition of the following compounds: malate and glutamate (5 mM), succinate (5 mM), ADP (10 mM), and antimycin-A (8 μM). For MAO-B-specific H_2O_2 emissions, baseline fluorescence was measured prior to the addition of two boluses of 20 μM 2-phenylethylamine and 10 μM rasagiline (Sigma). Rates of mitochondrial H_2O_2 production were calculated as the change in fluorescence per minute after subtraction of baseline, and results are presented as fold change from the digitonin condition. Rates of MAO-B-specific H_2O_2 emissions were calculated as the rasagiline-sensitive change in fluorescence per minute.

2.8. High resolution respirometry and membrane potential analyses

For the analysis of mitochondrial function in differentiated SH-SY5Y cells, high-resolution respirometry was conducted using an Oxygraph-2k system (OROBOROS Instruments, Innsbruck, Austria) at 37 °C with a constant stirring speed of 750 rpm. Harvested cells were counted, and resuspended in mitochondrial respiration medium, MiRO5 (0.5 mM EGTA, 3 mM $MgCl_2$–$6H_2O$, 20 mM taurine, 10 mM K_2HPO_4, 20 mM HEPES, 110 mM sucrose, and 1 g/L BSA; pH 7.1 at 37 °C). Resting respiration was measured in intact cells prior to permeabilization with

4.05 μM digitonin. The SUIT protocol involved consecutive additions of 2 mM malate, 5 mM pyruvate, 10 mM glutamate, 5 mM ADP (complex I phosphorylating respiration), 10 mM succinate (complex I- and complex II- phosphorylating respiration), and 0.25 μM titrations of carbonyl cyanide p-trifluoromethoxyphenyl hydrazine (FCCP; maximal uncoupled respiration). Non-mitochondrial respiration was measured after the addition of 2.5 μM antimycin A.

Fluorometric analysis of mitochondrial membrane potential ($\Delta\psi_m$) during HRR respiratory states was determined separately using tetramethyrhodamine methyl ester perchlorate (TMRM). The raw fluorescence signal was calibrated to μM TMRM, which represents the proportion of unaccumulated fluorescence signal in the mitochondrial matrix (inversely proportional to $\Delta\psi_m$). μM TMRM values were converted to $\Delta\psi_m$ (expressed in mV) using the following equation adapted from the Nernst Equation, which expresses $\Delta\psi_m$ as a function of μM TMRM:

$$\Delta\psi m\ (\mu M\ \mathrm{TMRM}) = 61.5 \times log_{10}\left(\frac{\frac{(inital\ C_{TMRM})\times(V_{total})}{\mu M\ \mathrm{TMRM}} \times 10^{-6} - (V_{total} - (V_m \times P_m) - (K_o' \times P_c))}{(V_m \times P_m) + (K_i' \times P_m)}\right)$$

Where *inital* C_{TMRM} is the initial concentration of TMRM, equal to $2\bullet10^{-6}$ M.

V_{total} is the total volume of the measurement chamber, equal to 2000 μL.

V_m is mitochondrial volume per mg weight, assumed to be 1 μL/mg.

P_c is the protein content in the chamber, estimated to be 1.607 mg/μL total for SH-EV cells and 0.6 mg/μL total for SH-Spike cells based on experimental determinations.

P_m is the mitochondrial protein content in the chamber, estimated to be 0.14 mg/μL total for both SH-EV and SH-Spike cells based on experimental determinations.

K_o' is the partition coefficient between the external medium and the inter-membrane surface of the mitochondrial inner membrane, assumed to be 88 μL/mg.

K_i' is the partition coefficient between the mitochondrial matrix volume and the matrix facing surface of the mitochondrial inner membrane, assumed to be 36 μL/mg

2.9. Protein extraction

SH-SY5Y cells were lifted using trypsin, harvested, and pelleted in cold 1x PBS. Pellets were stored at −80 °C for later use. Cell pellets were resuspended in lysis buffer (10 mM Tris-HCl pH 7.4, 150 mM NaCl, 0.5% *v/v* Triton X-100, and 1 mM EDTA) with 0.1% protease inhibitor cocktail (PIC) and lysed with a 28-gauge needle. Lysed cell homogenates were centrifuged at 14,000 g for 10 min at 4 °C, and supernatant without cellular debris was collected. Protein concentration was determined by a BCA-protein kit, as per the manufacturer's protocol (Thermo Fisher, 23225).

2.10. Enzyme activities

Citrate synthase (CS) and lactate dehydrogenase (LDH) activities were determined in cell homogenates as previously described (Pileggi et al., 2016). In brief, cell pellets were homogenized in ice-cold homogenization buffer (50 mM Tris HCl, 150 mM NaCl, 1 mM EDTA, 1% Triton X-100, pH 7.4) by mechanical lysis with a 28-gauge needle. Samples were subsequently centrifuged at 10,000 g for 10 min at 4 °C, and the supernatant was collected for enzymatic activities.

Complex I and Complex I + III-linked activities were determined on enriched mitochondrial fractions as previously described (Spinazzi et al., 2012). Protein levels were quantified using the Pierce™ BCA Protein Assay Kit (Thermo Fisher, 23225).

Rate of change of absorbance and path length of each well were determined, and enzyme activities were calculated using extinction coefficients of 6.22 mM−1 cm−1 for LDH and Complex I, 13.6 mM−1 cm−1 for CS, and 18.5 mM−1 cm−1 for Complex I + III-linked activity.

2.11. Extracellular lactate

For extracellular L-lactate quantification, 700,000 cells were seeded in T25 flask and differentiated for 7 days. Media was collected for analysis following 24 h of incubation using a commercially available lactate assay kit (Sigma-Aldrich) according to the manufacturer's instructions.

2.12. Mitochondrial to nuclear DNA quantification

DNA was extracted as previously described (Guo et al., 2009). DNA concentration and purity were verified using the NanoDrop™ 2000 UV–Vis spectrophotometer (Thermo Fisher). Mitochondrial DNA (mtDNA) to nuclear DNA (nDNA) ratios were determined through qPCR against mitochondrial DNA gene MT-ND1 (FWD: 5′- AACATACCCATGGCCAACCT -3′, REV: 5′- AGCGAAGGGTTGTAGTAGCCC -3′) and nuclear DNA gene 18SrRNA (FWD: 5′- TAGAGGGACAAGTGGCGTTC -3′, REV: 5′- CGCTGAGCCAGTCAGTGT -3′). Ten μL qPCR reactions were performed in triplicate using 1*X* SsoAdvanced™ Universal SYBR® Green Supermix (Bio-Rad), qPCR data was compiled using the CFX Maestro software (Bio-Rad) and analysed manually using the $2^{-\Delta\Delta CT}$ method. mtDNA:nDNA ratios are expressed relative to empty vector cells in each set of biological replicate samples.

2.13. Immunoblotting

Proteins were separated by SDS-PAGE under reducing conditions and transferred to PVDF membranes and incubated overnight with primary antibodies against: α-Tubulin (Sigma T6199, 1:5000), AIF (Abcam, ab32516, 1:2000), BAX (ProteinTech, 50,599). BCL-2 (ProteinTech, 12,789), BNIP3 (Abcam, ab10433), DRP-1 (BD Biosciences, 611113s), Fis1 (BioVision 3491), GPX4 (Abcam ab16800), HA (Cell Signaling, 3724), HIF1 (ProteinTech, 20960), LAMP1 (ProteinTech, 21997), LC3I/II (Cell Signaling, 12741s, 1:2000), MCL-1 (600-401-394, Rockland, 1:1000), MFF (Santa Cruz sc-168,593), MFN1/2 (Abcam, ab57602), MDM2 (ProteinTech, 27,883–1), NRF1 (Abcam, ab175932), NRF2 (Protein Tech, 16,396–1), OPA-1 (Abcam, 42,364), Total OXPHOS Human WB Antibody Cocktail (Abcam, ab110411), SOD1 (Santa Cruz sc-11407), SOD2 (Santa Cruz, sc-30080, 1:2000), p53 (Cell Signaling, 2524), p62 (Cell Signaling, 5114s, 1:2000), Parkin (Santa Cruz, sc-32282, 1:2000), PGC1α (ST1202, Millipore, 1:1000), TFAM (Abcam, ab131607) VDAC (Cell Signaling, 4661), and Vinculin (1:10,000, Abcam, ab129002). Protein bands were visualised using the Chem-iDoc™ MP Imaging System (Bio-Rad). Protein carbonyls were quantified using the OXYBLOT kit (Millipore), according to the manufacturer's protocol and transferred to nitrocellulose membranes. Densitometry band analysis was performed using Image J software. The abundance of target proteins is presented normalised to loading control (α-Tubulin, Vinculin) or Ponceau staining.

2.14. GSH and GSSG quantification by HPLC

GSH and GSSG were quantified by HPLC with an Agilent 1100 series HPLC as previously described (Liaghati et al., 2021).

2.15. Cell death and viability assays

SH-SY5Y cells were treated with 1.5 mM 1-methyl-4-phenyl-1,2,3,6-tetrahydropyridine, hydrochloride (MPTP, Santa Cruz, sc-206178) with and without 10 μM rasagiline (Sigma) for 24 h. Cell death and viability

assays were carried out using trypan blue exclusion and/or an Annexin V-FITC/PI Detection Kit (BD Biosciences, San Diego, CA, USA) according to the manufacturer's instructions. Briefly, 1×10^6 cells were resuspended in binding buffer, and subsequently stained with 5 μl Annexin V-FITC and 5 μl PI for 15 min. The samples were analysed with flow cytometry (BD FACSCelesta™ Cell Analyzer, BD Biosciences).

2.16. Statistical analysis

Statistical analysis was performed using Prism software (GraphPad Software Inc., La Jolla, California, USA). An unpaired two-tailed Student's t-test was used to determine statistical significance for comparisons between two groups (i.e., SH-Spike versus SH-EV). To assess the effect of MPTP-induced cell death, a two-way ANOVA was used with spike and MPTP as independent variables, followed by Holm-Sidak post hoc tests for multiple comparisons. Values less than 0.05 were considered statistically significant. Data are presented as means ± standard deviation (SD).

3. Results

3.1. SARS-CoV-2 spike glycoprotein (S protein) interacts with MAO-B

In silico mapping of SARS-CoV-2 interactions has revealed that sequence elements contained on the 5′ untranslated region of the SARS-CoV-2 viral genome can direct SARS-CoV-2 RNA to localize and interact with mitochondria (Wu et al., 2020). Protein-protein docking analysis and computational structural comparisons between MAO-B and ACE2 have indicated that the S protein may have a high binding affinity to MAO-B (Cuperlovic-Culf et al., 2021; Hok et al., 2022), suggesting that the S protein could interact and influence MAO-B activity. One of our primary aims was to establish if the S protein can interact with MAO-B *in situ*. To test this interaction, we first transfected HEK293T cells with an N-terminal FLAG-tagged SARS-CoV-2 Spike (FLAG-Spike), and/or C-terminal HA-tagged MAO-B (MAO-B-HA), or an empty vector (pcDNA3.1+). Visualisation of the transduced HEK293T cells with immunofluorescence confocal microscopy showed co-localization between the S protein and MAO-B (Fig. 1a).

To test whether S-protein interacts with MAO-B, we subsequently applied the highly sensitive proximity ligation assay (PLA), which produces a fluorescence signal when two proteins are in close proximity (<40 nm resolution) and thus represents single molecule protein interaction events (Gullberg and Andersson, 2010). Fluorescent puncta were not detected in HEK293T cells transfected with an empty vector (pcDNA3.1+), FLAG-SARS-CoV-2 spike only, or MAO-B-HA only (Fig. 1b), whereas the HEK293T cells co-transfected with both SARS-CoV-2 spike and MAO-B-HA did exhibit fluorescent puncta, confirming interactions between the S protein and MAO-B (Fig. 1b).

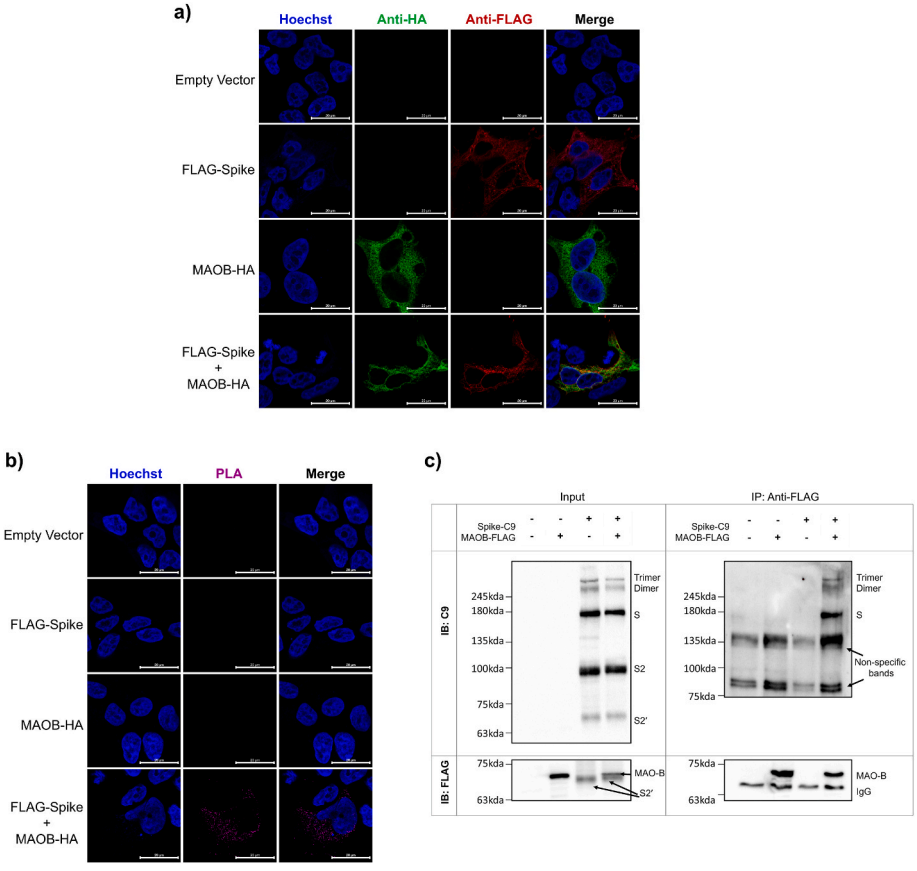

Fig. 1. SARS-CoV-2 spike glycoprotein interacts with MAO-B (a) HEK293T cells were transfected with plasmids encoding an empty pcDNA vector, MAO-B-HA, and/or FLAG-SARS-CoV-2 spike. Representative immunofluorescence staining of Hoechst-stained nuclei (blue), anti-HA (green), and anti-FLAG (red) are shown, scale bar = 20 μm. Colocalization was observed between MAO-B-HA and FLAG-SARS-CoV-2 spike, (n = 3, from independent experiments). (b) HEK293T cells were transfected with plasmids encoding an empty pcDNA vector, MAO-B-HA, and/or FLAG-SARS-CoV-2 spike. In situ proximity ligation assays (PLA) in transfected cells were performed using anti-HA and anti-FLAG antibodies, and the nuclei were stained with Hoechst, Scale bar = 20 μm, (n = 3, from independent experiments). (c) HEK293T cells were transfected with plasmids encoding an empty pcDNA vector, MAO-B-FLAG, and/or SARS-CoV-2 spike-C9. Immunoblots of input cells lysates (1% of IP input) and immunoprecipitates (IP) show that SARS-CoV-2 spike-C9 immunoprecipitates with MAO-B-FLAG, (n = 3, from independent experiments). See also Fig. S1 for colocalization between SARS-CoV-2 spike-C9 immunoprecipitates and MAO-B-FLAG. (For interpretation of the references to colour in this figure legend, the reader is referred to the Web version of this article.)

To establish direct interaction, we next transfected HEK293T cells with C-terminal FLAG-tagged MAO-B (MAO-B-C9), and/or a C-terminal C9-tagged SARS-CoV-2 spike (Spike-C9), or an empty pcDNA3.1+ vector, and observed co-localization between the S protein and MAO-B (Fig. S1). We then performed co-immunoprecipitation (Co-IP)-pulldown on HEK293T cells transfected with MAO-B-FLAG, and/or SARS-CoV-2 spike-C9, or pcDNA3.1+ vector. The S protein co-immunoprecipitated with MAO-B-FLAG pulldown (Fig. 1c), confirming that the S protein can bind to MAO-B. Of note, the S2 and S2' subunits observed in the input immunoblot were not observed in the IP blot as S2 does not contain the RBD.

3.2. Expression of the SARS-Cov-2 spike glycoprotein enhances MAO-B activity

We next sought to determine whether the S protein could influence mitochondrial metabolism and MAO-B activity in neuronal cells. MAO-B is highly expressed in dopaminergic neurons, which are permissive to SARS-CoV-2 infection (Yang et al., 2020). Human SH-SY5Y neuroblastoma cells stably expressing SARS-CoV-2 S protein fused with a C-terminal HA tag (SH-Spike) were generated through lentiviral transduction and subsequent selection. As a negative control, SH-SY5Y cells expressing an identical empty vector backbone (SH-EV) were generated through lentiviral transduction and selected with the same zeocin resistance. We confirmed stable expression of the S protein in SH-SY5Y cells using immunofluorescence and immunoblotting techniques (Fig. 2a and b). Stable expression of the S protein did not influence cell viability, as analysed by trypan blue exclusion (Fig. 2c).

The oxidation of monoamines by monoamine oxidases requiring water and oxygen yields an aldehyde product, hydrogen peroxide (H_2O_2), and ammonia. To test whether expression of the S protein influenced MAO-B activity, we used the highly specific MAO-B substrate, ^{14}C phenylethylamine, to determine whether the formation of 2-phenylacetaldehyde by MAO-B was affected (Tipton et al., 2000). In assays conducted in cell lysates, SH-Spike cells exhibited increased rates of 2-phenylacetaldehyde formation compared to SH-EV control cells, indicative of increased MAO-B activity (Fig. 2d). The enhanced rates of 2-phenylacetaldehyde formation by MAO-B were inhibited by rasagiline, an irreversible MAO-B inhibitor (Oldfield et al., 2007). We next performed the experiments in enriched mitochondrial fractions to account for potential differences in mitochondrial content and confirmed increased monoamine oxidation again in the mitochondrial fractions isolated from SH-Spike cells (Fig. 2e).

As H_2O_2 is generated by MAO-B, fluorometric determinations of H_2O_2 emissions can be quantified to assess MAO-B activity using benzylamine or 2-phenylethylamine as substrates (Tipton et al., 2000). SH-Spike cells demonstrated greater rasagiline-sensitive H_2O_2 emissions with 2-phenylethylamine as a substrate compared to the SH-EV control (Fig. 2f), again consistent with the conclusion that the S protein increases MAO-B activity.

3.3. Expression of the SARS-Cov-2 spike glycoprotein alters mitochondrial metabolism

Increased MAO-B activity contributes to neuronal mitochondrial dysfunction through the formation of ROS, which can depolarize the mitochondrial membrane potential and impair bioenergetic function (Kaludercic et al., 2014; Wei et al., 1996). Beyond mitochondrial functions, there is also mounting evidence that SARS-CoV-2 can alter cellular metabolism (Ajaz et al., 2021; Crunfli et al., 2022; de Oliveira et al., 2022; Shang et al., 2021). To investigate if the expression of the S protein influenced mitochondrial function, we first quantified markers of mitochondrial content. SH-Spike cells displayed higher citrate synthase activity (Fig. 3a) and mtDNA:nDNA (Fig. 3b) compared to SH-EV cells,

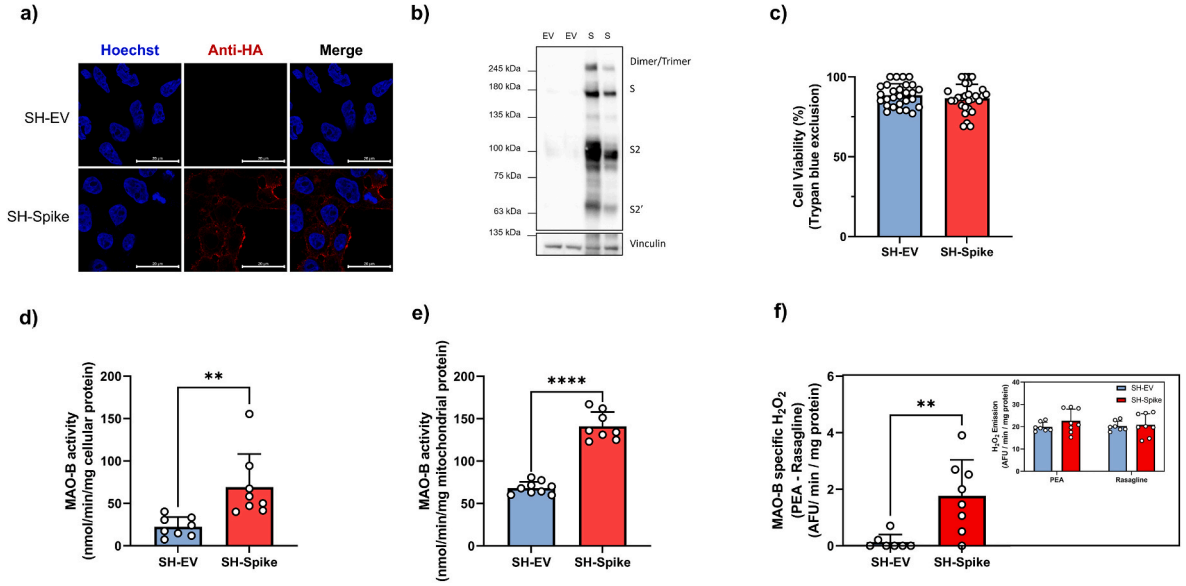

Fig. 2. SARS-CoV-2 spike glycoprotein increases MAO-B activity. (a) Generation of SH-SY5Y neuron-like cells stably expressing HA-tagged SARS-CoV-2 spike glycoprotein (SH-Spike) or an empty vector (SH-EV). Confocal microscopy of permeabilized cells stained for HA to detect spike (red) and Hoechst-stained nuclei (blue). (b) Immunoblotting analysis using anti-HA demonstrating that the SH-Spike cells express the full-length spike protein, (n = 12). (c) Cell viability did not differ between SH-SY5Y cells expressing the SARS-CoV-2 spike glycoprotein or the EV, as assessed by trypan blue exclusion (n = 28). **(d–e)** MAO-B catalytic activity was measured using ^{14}C-phenylethylamine in cells and in isolated mitochondria of SH-Spike and SH-EV cells. MAO-B specific oxidation was determined using the MAO-B inhibitor, rasagiline. SARS-CoV-2 spike expression increased the rate of MAO-B-specific oxidation of 2-phenylethylamine to 2-phenylacetaldehyde in **(d)** whole cells, and **(e)** mitochondria isolated from SH-Spike cells (cells n = 8; isolated mitochondria n = 9 SH-EV, n = 8 SH-Spike). **(f)** MAO-B-specific H_2O_2 emissions were quantified in SH-Spike and SH-EV cells using phenylethylamine (PEA) as a substrate in the presence of Amplex Red in a spectrofluorometer. Specificity was determined using rasagiline, an MAO-B inhibitor. SARS-CoV-2 spike expression in SH-SY5Y cells increased MAO-B specific H_2O_2 emissions, (n = 7 SH-EV, n = 8 SH-Spike). Inset depicts H_2O_2 emissions in response to PEA and rasagiline used to determine MAO-B specific H_2O_2 emissions. (d) Comparisons between groups were determined using a two-tailed Student's t-test. Values are mean ± SD. $^*P < 0.05$, $^{**}P < 0.01$, $^{***}P < 0.001$. (For interpretation of the references to colour in this figure legend, the reader is referred to the Web version of this article.)

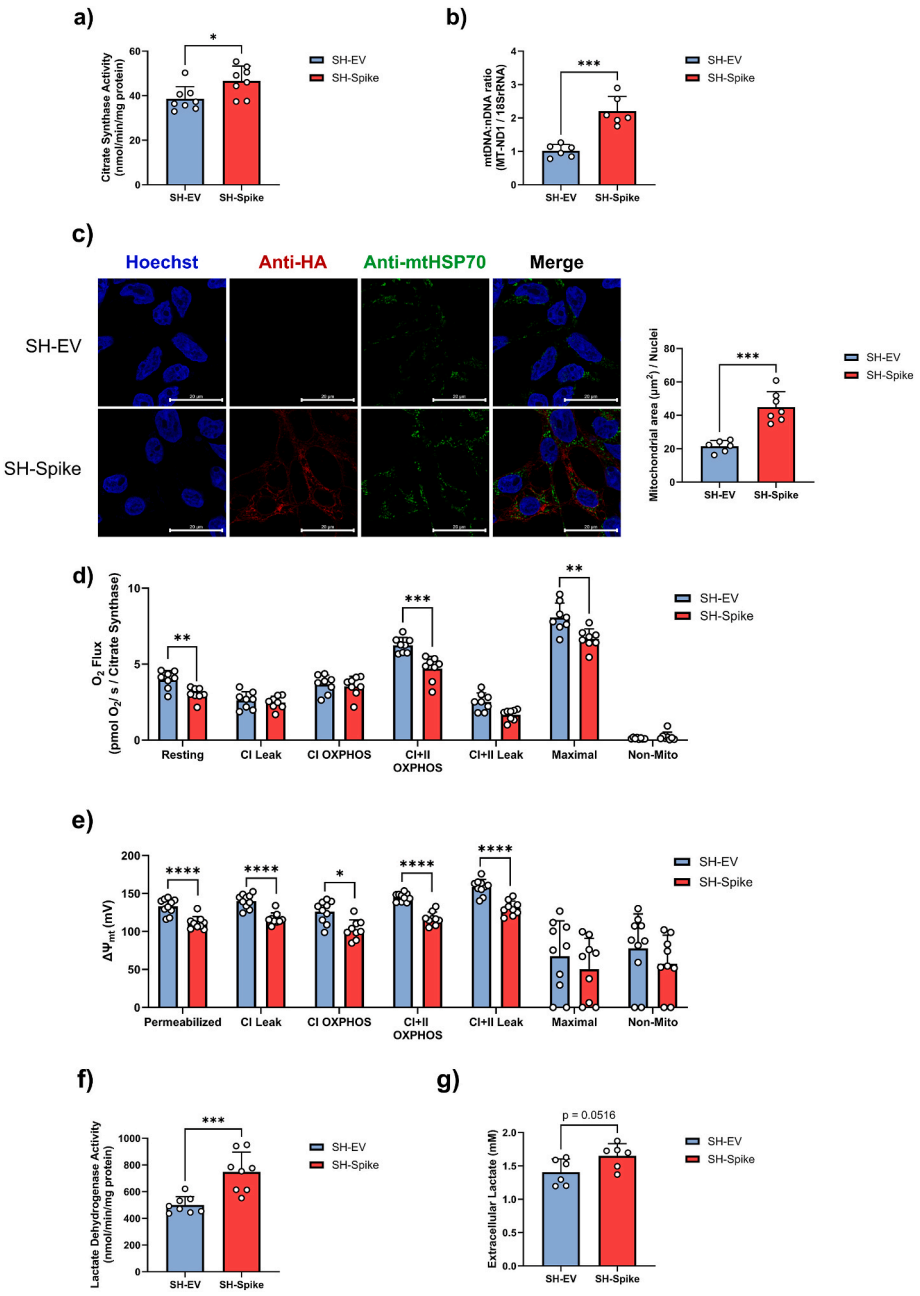

Fig. 3. SARS-CoV-2 spike glycoprotein modifies mitochondrial bioenergetics. **(a–c)** SH-SY5Y cells expressing the SARS-CoV-2 spike glycoprotein (SH-Spike) have increased mitochondrial content compared to SH-SY5Y cells expressing an empty vector (SH-EV). **(a)** Citrate synthase activity (n = 8), and **(b)** mtDNA:nDNA were higher in SH-Spike cells compared to SH-EV (n = 6). **(c)** Confocal microscopy of SH-Spike (HA-tagged) and SH-EV cells stained for anti-mtHSP70, anti-HA, and nuclei (Hoechst). Mitochondrial area per nuclei was greater in SH-Spike cells compared to SH-EV (n = 6 SH-EV, n = 7 SH-Spike). (d) High resolution respirometry of SH-SY5Y cells expressing the SARS-CoV-2 spike glycoprotein (SH-Spike) or an empty vector (SH-EV). Resting, maximal, and complex I + II OXPHOS respiration rates normalised to citrate synthase (CS), a marker of mitochondrial content, were lower in SH-Spike cells compared to SH-EV (n = 8). (e) Fluorometric quantification of mitochondrial membrane potential (ΔΨm). Mitochondrial membrane potential was lower in SH-Spike cells compared to SH-EV (n = 10 SH-EV, n = 9 SH-Spike; n = 8 SH-EV and n = 7 SH-Spike for maximal and non-mitochondrial membrane potential). (f) Lactate dehydrogenase activity was higher in SH-Spike cells compared to SH-EV (n = 8). (g) Lactate measured in extracellular media after 24 h was higher in SH-Spike cells compared to SH-EV (n = 6). Comparisons between groups were as determined using a two-tailed Student's t-test. Values are mean ± SD. *$P < 0.05$, **$P < 0.01$, ***$P < 0.001$.

indicative of increased mitochondrial content. Immunocytochemical staining of mtHSP70 revealed that SH-Spike expression increased mitochondrial area (normalised to the number of nuclei) compared SH-EV (Fig. 3c), again consistent with elevated mitochondrial content.

We subsequently conducted high-resolution respirometry on digitonin-permeabilized SH-SY5Y neuron-like cells to examine detailed characteristics of mitochondrial bioenergetics. Expression of the S protein did not affect Complex I + II- driven OXPHOS, oligomycin-induced Complex I + II -driven leak respiration, FCCP-induced maximal respiration, or non-mitochondrial respiration (Fig. S2). In contrast, the SH-Spike cells displayed enhanced complex I-driven OXPHOS compared to SH-EV neuronal cells (Fig. S2). Complex I-driven leak respiration also tended to be higher in SH-Spike cells (p = 0.067, Fig. S2). However, upon normalisation to citrate synthase to account for elevations in mitochondrial content, we observed lower resting respiration of intact cells (i.e., prior to permeabilization), as well as lower Complex I + II-

driven OXPHOS, Complex I + II-driven leak respiration, and FCCP-induced maximal respiration in permeabilized SH-SY5Y cells (Fig. 3d), consistent with the conclusion that the S protein impairs intrinsic mitochondrial bioenergetic functions. Spectrophotometric assessments of maximal catalytic activity of electron transport chain complexes revealed no difference in rotenone-sensitive complex I activity in isolated mitochondria from SH-Spike and SH-EV neuron-like cells (Fig. S2), and instead showed that Complex I + III-linked activity was decreased in SH-Spike cells (Fig. S2). Moreover, fluorometric-based analysis of mitochondrial membrane potential with TMRM revealed that mitochondria in SH-Spike cells were depolarized across different respiratory states (Fig. 3e), again consistent with impaired mitochondrial bioenergetic functions.

Increases in glycolysis have been observed in patient PBMCs and SARS-CoV-2-infected monocytes (Ajaz et al., 2021; Codo et al., 2020), suggesting that SARS-CoV-2 infection may elicit the Warburg effect. As a proxy measure of anaerobic metabolism, we next quantified LDH activity and extracellular lactate concentrations. Consistent with a shift in oxidative to glycolytic metabolism, SH-SY5Y-Spike cells demonstrated increased LDH activity and higher lactate concentrations in cultured medium compared to SH-EV cells (Fig. 3f and g).

3.4. SARS-CoV-2 spike glycoprotein increases oxidative stress

The exacerbated inflammatory response that occurs with SARS-CoV-2 infection is associated with the upregulation of ROS production through the MAVS/TRAF3/TRAF6 signalosome (Lage et al., 2021). To evaluate if the S protein could elicit increased mitochondrial ROS production, fluorometric-based analysis of H_2O_2 emission was conducted on digitonin permeabilized cells. H_2O_2 emission was higher in SH-Spike cells in the presence of succinate (i.e., energized non-phosphorylating condition), ADP (i.e., energized phosphorylating condition), and antimycin (i.e., inhibited electron transport chain condition), compared to SH-EV cells (Fig. 4a).

Protein expression of the superoxide dismutase enzymes (SOD1 and SOD2) did not differ between EV and S-expressing neuronal cells, suggesting that the detoxification of superoxide anions ($O_2^{\bullet-}$) remained unchanged with S protein expression. In contrast, the expression of glutathione peroxidase 4 (GPX4) was lower in SH-Spike expressing neuron-like cells (Fig. 4b), indicating that glutathione redox may be perturbed. Direct assessment of glutathione redox revealed that both reduced glutathione (GSH) and total glutathione (GSH + 2GSSG) were lower in SH-Spike cells, whereas oxidized glutathione (GSSG) and the ratio of GSH:GSSG were not different compared to SH-EV cells (Fig. 4c). Despite evidence of increased ROS production and altered glutathione redox, quantification of protein carbonylation revealed no difference between SH-Spike and SH-EV cells (Fig. 4d), consistent with impaired redox balance (redox stress) but not oxidative damage.

3.5. SARS-CoV-2 spike suppresses parkin expression and perturbs mitophagy

Mitochondrial content is governed by the tightly regulated processes of biogenesis and mitophagy, with the intricate balance between fusion and fission allowing for the dynamic remodelling of the mitochondrial network. We sought to assess if the apparent increase in mitochondrial content was due to elevated mitochondrial biogenesis or perturbed mitochondrial turnover. Immunoblotting of key mitochondrial transcription factors revealed decreases in PGC1a and NRF1 protein expression in SH-Spike cells, consistent with lower mitochondrial biogenesis, whereas NRF2 and TFAM did not differ between SH-EV and SH-Spike cells (Fig. 5a). Markers of mitochondrial fusion, OPA-1 and MFN1/2, and of mitochondrial fission, Fis1 and MFF, did not differ between SH-EV and SH-Spike cells (Fig. 5b and c), whereas fission protein DRP-1 was elevated in SH-Spike cells (Fig. 5c). Following oxidative stress and depolarization, DRP-1 acts to eliminate damaged mitochondria by forming multimeric ring-like structures to constrict and sever a budding mitochondrion (Kamerkar et al., 2018; Smirnova et al., 2001; Twig et al., 2008).

Damaged mitochondria can undergo PINK1/Parkin-mediated mitophagy as a protective measure to prevent cell death (Kim et al., 2007; Youle and Narendra, 2011). Thus, to test whether the increase in mitochondrial content in SH-Spike cells was due to altered mitochondrial turnover, we first quantified the expression of key autophagic proteins. LC3II/I expression did not differ between SH-EV and SH-Spike cells (Fig. 5d), suggesting that autophagy remains intact. In contrast, parkin expression was decreased by ~32% in SH-Spike cells (Fig. 5d). Parkin is a cytosolic E3 ubiquitin ligase that is recruited to the mitochondrial membrane by PINK1 to ubiquitinate proteins on the outer mitochondrial membrane, such as VDAC and MFN2. The accumulation of polyubiquitinated outer membrane proteins attracts p62, an adaptor protein that initiates autophagosome encapsulation of the mitochondria.

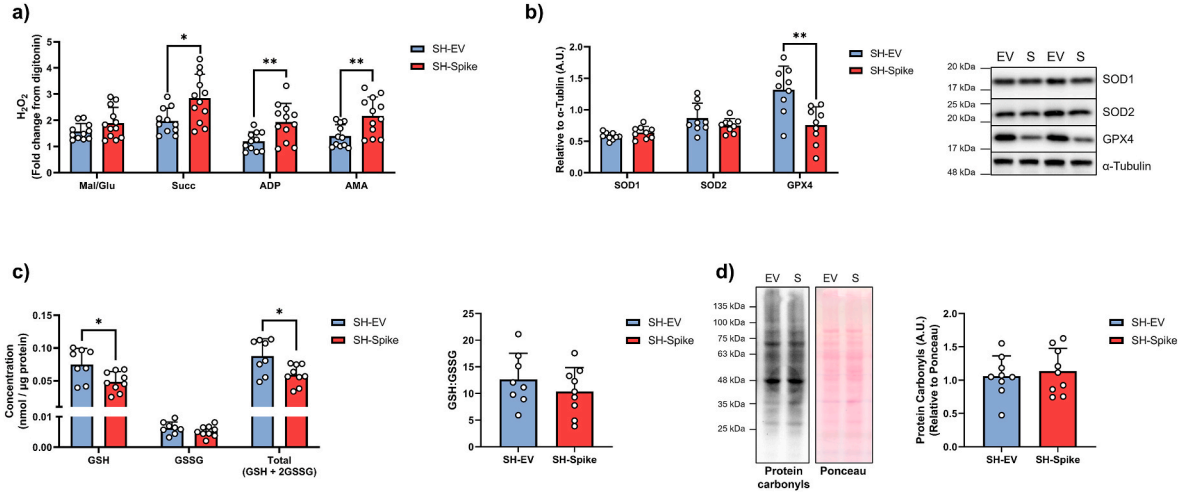

Fig. 4. SARS-CoV-2 spike glycoprotein increases oxidative stress in SH-SY5Y cells. (a) H_2O_2 emissions in digitonin-permeabilized SH-SY5Y cells was higher in SH-Spike cells (n = 11 SH-EV, n = 12 SH-Spike). (b) Immunoblotting of antioxidant enzymes, SOD1 or SOD2, revealed no differences. SARS-CoV-2 spike glycoprotein expression in SH-SY5Y cells decreased GPX4 protein expression (n = 9). (c) Total glutathione and reduced glutathione concentrations were lower in SH-Spike cells compared to SH-EV (n = 8 SH-EV, n = 9 SH-Spike). (d) Protein carbonyls did not differ between SH-Spike and SH-EV cells (n = 9). Comparisons between groups were determined using a two-tailed Student's t-test. Values are mean ± SD. *$P < 0.05$, **$P < 0.01$, ***$P < 0.001$.

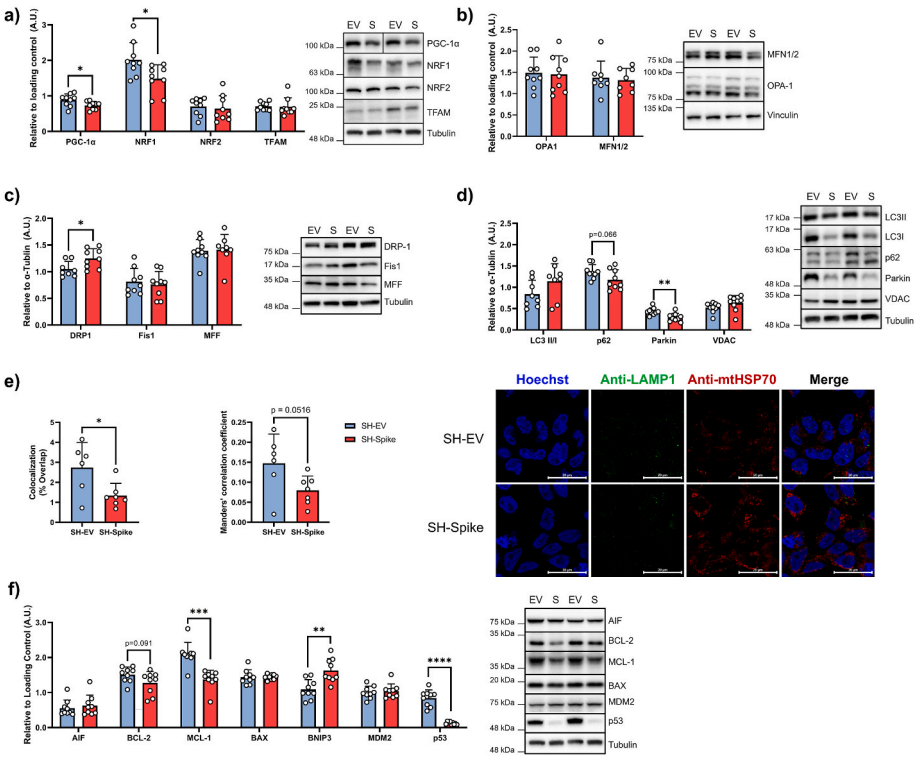

Fig. 5. SARS-CoV-2 spike glycoprotein perturbs mitophagy and decreases expression of mitochondrial transcription factors. (a) Immunoblot quantification of mitochondrial transcription factors. Expression of PGC1a and NRF1 were decreased in SH-Spike cells, whereas NRF2 and TFAM expression did not differ compared to SH-EV cells (n = 8–9). (b) Immunoblot quantification of mitochondrial fusion proteins. Expression of OPA-1 and MFN1/2 did not differ between SH-Spike and SH-EV cells (n = 8–9). (c) Immunoblot quantification of mitochondrial fission proteins. DRP-1 expression was elevated in SH-Spike cells compared to SH-EV, whereas Fis1 and MFF expression levels were similar between groups (n = 8–9). (d) Immunoblot quantification of mitophagy and autophagy proteins. Expression of LC3II/I and VDAC were similar between groups, whereas parkin and p62 were lower in SH-Spike cells compared to SH-EV (n = 8–9). (e) Confocal microscopy of SH-Spike (HA-tagged) and SH-EV cells stained for anti-mtHSP70, anti-LAMP1, and nuclei (Hoechst). Quantification of mitochondria and lysosomes using Mander's correlation coefficient (0 = no colocalization, 1 = full colocalization) and % overlap demonstrates less colocalization between mitochondria and LAMP1 (n = 6 SH-EV, n = 7 SH-Spike). (f) Immunoblot quantification of proteins regulating apoptosis. BNIP3 expression was higher in SH-Spike cells, whereas BAX, AIF, and MDM2 expression were similar between groups. In contrast, expression of MCL-1 was lower in SH-Spike cells compared to SH-EV. BCL-2 expression also tended to be lower in SH-Spike cells, and there was a dramatic decrease in p53 expression in SH-Spike cells (n = 8–9). Comparisons between groups were determined using a two-tailed Student's t-test, unless otherwise stated. Values are mean ± SD. *$P < 0.05$, **$P < 0.01$, ***$P < 0.001$.

While VDAC expression did not differ between SH-Spike and SH-EV, p62 tended to be lower in SH-Spike cells (p = 0.066; Fig. 5d), consistent with previous reports of impaired p62-mediated mitochondrial encapsulation into autophagosomes (Shang et al., 2021). We next performed immunocytochemical staining with mtHSP70 and lysosomal-associated membrane protein 1 (LAMP1) to quantify the colocalization of mitochondria and lysosomes. Semi-automated analysis of the acquired images revealed a decrease in the percent of mitochondria colocalized with LAMP1 in SH-Spike compared to SH-EV cells, with a strong trend in the Manders' colocalization coefficient (p = 0.0516, Fig. 5e).

With converging evidence suggesting that mitophagy is impaired in SH-Spike cells, we next sought to determine if SH-Spike cells had enhanced susceptibility to cell death. Mitochondria play an integral role in apoptotic cell death by releasing mitochondrial proteins such as cytochrome *c* and apoptosis-inducing factor (AIF) into the cytosol to activate caspases when pro-apoptotic factors induce mitochondrial outer membrane permeabilization (Green and Kroemer, 2004). We first quantified the expression of key proteins involved in the regulation of apoptosis. Protein expression of the anti-apoptotic factor MCL-1 was ~34% lower in SH-Spike cells and BCL-2 tended also to be lower compared to SH-EV cells (p = 0.091, Fig. 5f); however, expression of pro-apoptotic factors BAX and apoptosis-inducing factor (AIF) expression did not differ between groups (Fig. 5f). In contrast, BCL-2 and adenovirus E1B 19 kDa-interacting protein 3 (BNIP3) protein expression was higher in SH-Spike cells (Fig. 5f). Importantly, BNIP3 participates in both mitophagy and apoptosis by initiating mitochondrial encapsulation into autophagosomes through direct interactions with LC3-II (Hanna et al., 2012), as well as inducing opening of the mitochondrial permeability transition pore (mPTP) and cytochrome *c* release to activate apoptotic and autophagic responses (Diwan et al., 2007; Kim et al., 2002; Kubasiak et al., 2002; Kubli et al., 2007; Velde et al., 2000). The expression of MDM2, a negative regulator of p53, did not differ between groups (Fig. 5f), but there was a dramatic ~85% decrease in p53 protein expression in SH-Spike cells (Fig. 5f).

3.6. *SARS-CoV-2 spike increases susceptibility to 1-methyl-4-phenyl-1,2,3,6- tetrahydropyridine (MPTP)-induced neuronal necrosis*

Lastly, we employed an *in vitro* model of Parkinson's disease where SH-Spike and SH-EV cells were challenged with 1-methyl-4-phenyl-1,2,3,6- tetrahydropyridine (MPTP) to induce cell death. MPTP is a potent neurotoxin that is oxidized to MPP^+ by MAO-B in a two-step process in astrocytes and serotonergic neurons. MPP^+ is the active neurotoxin that is transported into dopaminergic neurons, which accumulates within the inner mitochondrial membrane and inhibits complex I of the electron transport chain (Heikkila et al., 1984; Javitch et al., 1985; Ramsay and Singer, 1986). Following 24 h of treatment, trypan blue exclusion tests revealed that MPTP elicited cell death in SH-Spike cells, which was partially reversed with rasagiline (Fig. 6a). To discriminate between apoptosis and necrosis, flow cytometry analyses of cells stained with propidium iodine (PI) and annexin V (AnnV) demonstrated that SH-Spike cells exhibited a higher proportion of PI

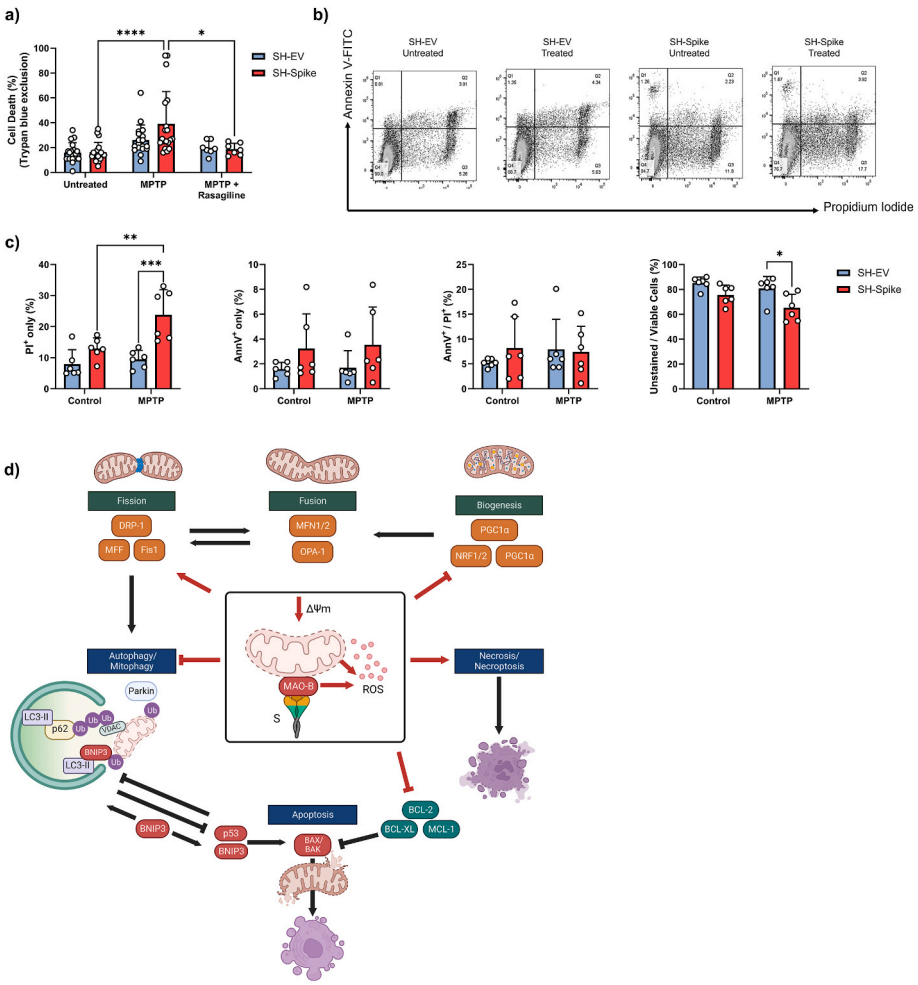

Fig. 6. The SARS-CoV-2 spike glycoprotein increases sensitivity to cell death. **(a–c)** SH-EV and SH-Spike cells were treated with 1.5 mM MPTP for 24 h. (a) Analysis of cell viability by trypan blue exclusion demonstrated that the MPTP treatment elicited cell death in SH-Spike cells, which was partially reserved by co-treatment with rasagiline (n = 7–12). (b) Flow cytometric analysis of cells stained with annexin V-fluorescein 5-isothiocyanate (FITC)/propidium iodide (PI) showed an increase in susceptibility to MPTP-induced necrotic cell death (n = 6). Representative density plots of cells stained with annexin V-fluorescein 5-isothiocyanate (FITC)/propidium iodide (PI) and analysed by flow cytometry. (c) The proportion of PI-positive cells was higher in SH-Spike cells following 24 h of MPTP treatment, whereas the proportion of live, unstained cells was lower in SH-Spike cells following 24 h of MPTP treatment, consistent with decreased cell viability. In contrast, the proportion of annexin V-FITC positively stained cells, and the proportion of cells positively stained with both PI/annexin V-FITC were similar between SH-EV and SH-Spike cells regardless of MPTP treatment. (d) Schematic summary of the SARS-CoV-2 spike glycoprotein-induced impairments in mitochondrial health that contribute to increased susceptibility to MPTP-induced cell death. Red lines indicate changes induced by expression of the SARS-CoV-2 spike glycoprotein in SH-SY5Y neuron-like cells. The S protein depletes mitochondria membrane potential and enhances MAO-B activity and ROS production. Expression of mitochondrial transcription factors are lower in neuron-like cells expressing the S protein. Degradation of depolarized mitochondria by mitophagy is inhibited, in part by lower expression of the E3 ligase, parkin, leading to the accumulation of depolarized aberrant mitochondria. Low expression of BCL-2 anti-apoptotic proteins and activation of necrosis/necroptosis increases the susceptibility to cell death. Comparisons between groups with a two-way ANOVA with Holm-Sidak post-hoc test. Values are mean ± SD. $*P < 0.05$, $**P < 0.01$, $***P < 0.001$. (For interpretation of the references to colour in this figure legend, the reader is referred to the Web version of this article.)

positive cells and a lower proportion of unstained cells compared to SH-EV cells (Fig. 6b and c), consistent with increased necrotic cell death. In contrast, the proportion of AnnV positively stained cells did not differ between SH-EV and SH-Spike cells regardless of MPTP treatment, suggesting that apoptosis was not induced (Fig. 6c). The observed increase in PI positive cells and the absence of changes in AnnV positive cells in SH-Spike cells suggests that necrotic cell death is induced in response to MPTP treatment rather than apoptotic cell death. Taken together, these data support a synergistic effect between MAO-B and the S glycoprotein in increased susceptibility to MPTP-induced cell death (summarized in Fig. 6d).

4. Discussion

SARS-CoV-2 is associated with neurocognitive symptoms that can persist following recovery from the initial infection. Emerging evidence suggests that SARS-CoV-2 may also be linked to post-encephalitic Parkinsonism (Smeyne et al., 2022), however, the molecular mechanisms are poorly elucidated. Persistent circulating S protein is associated with post-acute COVID-19 (Swank et al., 2023), and the spike glycoprotein can elicit alterations in cellular metabolism that may contribute to neurodegeneration (Clough et al., 2021; Lei et al., 2021). Here, we show that the S protein can interact with, and increase activity of MAO-B. We also demonstrate that the spike glycoprotein can impair mitochondrial bioenergetics, induce oxidative stress, perturb the degradation of depolarized aberrant mitochondria, and increase sensitivity to MPTP-induced cell death, which are common pathophysiological mechanisms shared with neurodegenerative diseases.

Progressive loss of nigrostriatal dopaminergic neurons in the substantia nigra pars compacta, and the accumulation of misfolded α-synuclein leading to Lewy body pathology are the hallmark features of Parkinson's disease. MAO-B activity is elevated in patients with

Parkinson's disease, and the high MAO-B activity results in increased dopamine catabolism and the formation of DOPAL, which plays a role in the aggregation of α-synuclein (Burke et al., 2008). As such, MAO-B inhibitors are an effective treatment to alleviate the motor symptoms of Parkinson's disease. Substantial brain invasion of SARS-CoV-2 is relatively uncommon, likely due to low ACE2 receptor expression in the brain; however, spatial distribution analysis of publicly available brain transcriptome databases revealed that ACE2 expression is relatively high in specific brain regions, including the substantia nigra (Chen et al., 2021). SARS-CoV-2 preferentially infects astrocytes (Crunfli et al., 2022), which also have high MAO-B expression and contribute to Parkinson's disease pathology (Mallajosyula et al., 2008). The SARS-CoV-2 S^1 subunit can readily cross the BBB, resulting in widespread brain regional distribution (Rhea et al., 2021). The new onset of Parkinsonism following SARS-CoV-2 infection has been reported in case studies along with presynaptic nigrostriatal dopamine disturbance (Cohen et al., 2020; Faber et al., 2020) and depigmentation of the substantia nigra (Kantonen et al., 2020). Patients with existing Parkinson's disease often need to increase the dosing of levodopa following SARS-CoV-2 infection (Antonini et al., 2020), indicating that SARS-CoV-2 infection is associated with elevated dopamine metabolism. Key pathways of neurodegeneration and Parkinson's disease were the top enriched pathways of differentially expressed proteins in proteomic analysis of post-mortem brain tissue from deceased COVID-19 patients (Crunfli et al., 2022). Our findings indicate that the S protein may contribute to neurodegeneration through increases in monoamine metabolism and interactions with MAO-B. Initially, the S protein was thought to interfere with the substrate entrance to the MAO-B active site (Cuperlovic-Culf et al., 2021). However, additional modelling by Hok et al. suggests that the SARS-CoV-2 spike protein modifies the electrostatic environment of the substrate binding site for MAO-B (Hok et al., 2022). Moreover, mutant SARS-CoV-2 variants have different ACE2 binding affinities, suggesting that the different SARS-CoV-2 strains may have varying degrees of activation or inhibition of MAO-B activity. The effects of certain spike variants on MAO-B activity may therefore depend on the surrounding environment such as proximity to lipid membranes. Future studies should experimentally determine MAO-B substrate binding affinity when complexed with various spike protein variants, both biochemically and in the context of living systems.

Alterations to monoamine metabolism with SARS-CoV-2 infection may also partly be amplified by the downregulation of L-DOPA decarboxylase (DDC) (Mpekoulis et al., 2021), which catalyzes L-DOPA to dopamine and, to a lesser degree, l-5-hydroxytryptophan to serotonin (Bertoldi, 2014). Altered monoamine metabolism may be of particular importance in severe cases of SARS-CoV-2 infection, as high plasma concentrations of homovanillic acid, an end-stage product of catechol-O-methyltransferase and monoamine oxidase metabolism, during infection was identified as a predictor of mortality (Richard et al., 2022). Increased metabolism of other monoamine substrates has also been observed. Specifically, levels of serotonin were found to be lowest in serum from patients with severe COVID-19, consistent with the possibility that the activity of MAOs may increase with increasing severity of COVID-19 disease (Saito et al., 2022; Shen et al., 2020). Importantly, since our analysis was limited to SH-SY5Y neuroblastoma cells with PEA as a substrate, the increase in MAO-B activity should be verified in other brain cell types and with other monoamine substrates.

Persistent expression of the spike glycoprotein has been detected in circulation and in enriched plasma neuron- and astrocyte-derived extracellular vesicles following acute COVID-19 recovery, and correlate with neuropsychiatric manifestations associated with long COVID (Peluso et al., 2022; Swank et al., 2023). High MAO-B activity and specific MAO-B polymorphisms are also associated with depression and chronic fatigue syndrome (Moriguchi et al., 2019; Smith et al., 2006), in part due to decreases in monoamine availability. Thus, our data indicating that MAO-B activity is elevated in the presence of the spike glycoprotein suggests certain individuals may be more sensitive to developing the neuropsychiatric symptoms associated with long COVID due to genetic differences. High levels of psychological distress prior to SARS-CoV-2 infection are associated with long-COVID neuropsychiatric symptoms, such as fatigue and 'brain fog', that impair routine daily activities (Wang et al., 2022).

The metabolism of monoamine substrates by MAO-B is directly linked to H_2O_2 production (Pizzinat et al., 1999), which can impair mitochondrial function and promote dopaminergic neuron cell death. Our findings of increased cellular complex-I linked respiration, which was attributable to greater mitochondrial content, is consistent with previous observations of increased respiration in SARS-CoV-2-infected astrocytes (Crunfli et al., 2022). Transcriptome profiling has revealed that SARS-CoV-2 downregulates transcript expression of nuclear-encoded mitochondrial genes, including those related to complex I (Miller et al., 2021). Decreased gene expression of complex I genes may be a compensatory mechanism as complex I is a major site of ROS production (Turrens, 1997). In agreement with this observation, cells expressing the spike glycoprotein displayed elevated rates of mitochondrial H_2O_2 emissions and lower glutathione content (GSH + 2GSSG). The observed decreases in glutathione in SH-Spike cells in our study could be a result of decreased glutathione synthesis, formation of various forms of thiol conjugates, and/or increased glutathione efflux via the multidrug resistance-associated protein 1 (MRP1) (Dringen and Hirrlinger, 2003; Hirrlinger et al., 2001). In support of this, depletion of cellular thiols in SARS-CoV-2-infected Vero-E6 cells has been attributed to both decreased *de novo* glutathione biosynthesis due to low availability of cysteine, and also increased glutathione efflux via increased MRP1 protein expression (Bartolini et al., 2021). Low endogenous levels of glutathione are thought to underlie severe SARS-CoV-2 infection (Kumar et al., 2021; Polonikov, 2020), and associate with white matter hyperintensities in the anterior cingulate cortex in COVID-19 survivors (Poletti et al., 2022). As oxidative stress is a major contributor to neurodegeneration in Parkinson's disease (Jiang et al., 2016), SARS-CoV-2 spike-induced increases in both MAO-B and mitochondrial ROS production may contribute to neurodegeneration following SARS-CoV-2 infection.

The apparent intrinsic impairment in mitochondrial function in the neuronal cells expressing the S protein is consistent with previously reported impairments in mitochondrial function in peripheral blood mononuclear cells (PBMCs) from patients with SARS-CoV-2 infections (Ajaz et al., 2021; Gibellini et al., 2020), and brain endothelial cells treated with recombinant SARS-CoV2 spike glycoprotein (Kim et al., 2021). Similarly, spike-induced elevations in ROS production have also been observed in microglia treated with recombinant S protein (Clough et al., 2021), and SARS-CoV-2 infection-induced loss of mitochondrial membrane potential has been observed in several tissues and different cell types (Ajaz et al., 2021; Romão et al., 2022; Shang et al., 2021). Examination of mitochondrial morphology in electron micrographs of astrocytes infected with SARS-CoV-2 has also revealed augmented mitochondrial fragmentation (de Oliveira et al., 2022), demonstrating the persistence of dysfunctional mitochondria. Elevations in mitochondrial content and increases in mtDNA have also been observed in mechanistic studies on SARS-CoV-2, with reports of time-dependent increases in mitochondrial volume and fragmentation (Flynn et al., 2021). Damaged cells release mtDNA into circulation to activate inflammation and neutrophil recruitment when a cell is unable to complete the removal of dysfunctional mitochondria via mitophagy (Caielli et al., 2016). Increased circulating mtDNA is a predictor of mortality in patients with severe COVID-19 (Harrington et al., 2019), consistent with mitochondrial dysfunction.

Our findings of elevated mitochondrial content without an increase in mitochondrial biogenesis support our conclusion that mitochondrial clearance is perturbed, leading to the accumulation of aberrant mitochondria. This observation extends the finding that dysfunctional mitochondria fail to be encapsulated into autophagosomes in SARS-CoV-2 infected Vero E6 cells (Shang et al., 2021) by demonstrating that the

spike glycoprotein may contribute to impaired mitophagy through decreased parkin-mediated ubiquitination of mitochondrial outer membrane proteins. The observed decrease in parkin expression may also contribute to enhanced MAO-B activity, as parkin can suppress the expression of MAO-B (Jiang et al., 2006). The drastic reduction of p53 in cells expressing the S protein may contribute to impaired mitophagy and elicit the Warburg effect by decreasing parkin expression (Zhang et al., 2011), which is supported by our findings of increased LDH activity and extracellular lactate. Computational modelling suggests that the SARS-CoV-2 S^2 subunit can interact with p53 and modulate its expression (Singh and Singh, 2020), which may be a mechanism to suppress type I interferon antiviral responses (Yuan et al., 2015).

Despite the marked reduction in p53 expression, our results show that the S protein can enhance the susceptibility to MPTP-induced neurotoxicity. MAO-B catalyzes the oxidation of MPTP to MPP^+ in astrocytes prior to MPP^+ uptake into dopaminergic neurons (Heikkila et al., 1984; Javitch et al., 1985; Ramsay and Singer, 1986). Genetic increases in MAO-B levels increases free radical damage and sensitivity to MPTP-induced cell death (Wei et al., 1996), implicating a role for enhanced metabolism of MPTP to MPP^+ by MAO-B in neuron-like cells expressing the SARS-CoV-2 S protein. While mechanisms behind cell death induced by MPTP/MPP^+ have are not fully understood, low doses MPP^+ are traditionally thought to trigger apoptosis and higher doses of MPP^+ are thought to trigger necrosis and/or necroptosis (regulated necrosis) (Nicotra and Parvez, 2000). However, recent findings have challenged this paradigm as MPP^+ -induced cell death in SH-SY5Y cells was mainly found to be independent of p53 and apoptosis (Ito et al., 2017). Instead of apoptosis, several forms of necrotic programmed cell death are thought to be activated in response to MPP^+ -induced neurotoxicity, including necroptosis and ferroptosis, which may also engage members of the BCL-2 family (Ito et al., 2017; Kane et al., 1995; Tischner et al., 2012). Our results are consistent with previous findings that the S protein can promote cell death through increases in ROS in HEK293T cells (Li et al., 2021) and THP-1-like-macrophages (Barhoumi et al., 2021), as well as the NLRP3 inflammasome-mediated activation of PANoptosis (pyroptosis, apoptosis, and necroptosis) in cultured adipocytes treated with the SARS-CoV-2 spike S1 subunit (Frühbeck et al., 2021). Thus, our findings of increased ROS and greater sensitivity to MPTP-induced neurotoxicity in cells expressing the spike glycoprotein implicates a role for MAO-B in neurodegeneration during SARS-CoV-2 infection.

In summary, we demonstrate that the SARS-CoV-2 S protein can interact with MAO-B and increase monoamine oxidation and that it impairs mitophagy, leading to increased content of aberrant mitochondria. Human SH-SY5Y neuron-like cells expressing S protein also had increased susceptibility to cell death following a challenge with Parkinsonian neurotoxin. Together, these findings highlight the mechanisms that may cause SARS-CoV-2-induced neurodegeneration and alterations in monoamine metabolism. Further research is needed to determine if MAO-B inhibitors could be a useful to prevent or mitigate SARS-CoV-2-induced neurodegeneration.

Availability of data and materials

All data generated for this manuscript are presented in the main manuscript or additional supporting files.

CRediT authorship contribution statement

Chantal A. Pileggi: Conceptualization, Investigation, Formal analysis, Visualization, Writing - original draft, Writing - review & editing. **Gaganvir Parmar:** Conceptualization, Formal analysis, Investigation, Visualization, Writing - original draft, Writing - review & editing. **Hussein Elkhatib:** Investigation, Formal analysis, Writing - review & editing. **Corina M. Stewart:** Investigation, Writing - review & editing. **Irina Alecu:** Writing – review & editing. **Marceline Côté:** Writing – review & editing. **Steffany A.L. Bennett:** Writing – review & editing. **Jagdeep K. Sandhu:** Investigation, Writing – review & editing, Supervision. **Miroslava Cuperlovic-Culf:** Conceptualization, Resources, Writing – original draft, Writing – review & editing, Supervision, Funding acquisition. **Mary-Ellen Harper:** Conceptualization, Resources, Writing – original draft, Writing – review & editing, Supervision, Funding acquisition.

Declaration of competing interest

The authors declare that they have no known competing financial interests or personal relationships that could have appeared to influence the work reported in this paper.

Data availability

Data will be made available on request.

Acknowledgements

This research was supported by the National Research Council (NRC) of Canada (MCC and MEH), and by a University of Ottawa Research Chair in Mitochondrial Bioenergetics (MEH). The authors would like to thank the Flow Cytometry and Virometry Core facility and The Cell Biology and Image Acquisition Core facility at the University of Ottawa.

Abbreviation list

ACE2	angiotensin-converting enzyme 2
AIF	apoptosis inducing factor
AnnV	annexin V
BBB	blood-brain barrier
BAX	Bcl-2-associated X protein
BCL-2	B-cell lymphoma-2
CNS	central nervous system
DRP1	dynamin-1-like protein
Fis1	mitochondrial fission 1 protein
GPX4	glutathione peroxidase 4
GSH	reduced glutathione
GSSG	oxidized glutathione disulfide
LAMP1	lysosomal-associated membrane protein 1
LDH	lactate dehydrogenase
LC3B	MAP1 light chain 3
MAO-B	monoamine oxidase B
MFF	mitochondrial fission factor
MFN	mitofusin
mtHSP70	mitochondrial heat-shock protein 70
MPTP	1-methyl-4-phenyl-1,2,3,6- tetrahydropyridine
NRF1	nuclear regulatory factor 1
NRF2	nuclear regulatory factor 2
OPA1	optic atrophy 1
PI	propidium iodine
PINK1	PTEN-induced putative kinase 1
PGC1α	peroxisome proliferator-activated receptor γ coactivator-1α
ROS	reactive oxygen species
S	Spike glycoprotein
SARS-CoV-2	severe acute respiratory syndrome coronavirus 2
SOD	superoxide dismutase
TFAM	mitochondrial transcription factor A
VDAC	voltage-dependent anion channel

Appendix A. Supplementary data

Supplementary data to this article can be found online at https://doi.org/10.1016/j.crneur.2023.100112.

References

Ajaz, S., McPhail, M.J., Singh, K.K., Mujib, S., Trovato, F.M., Napoli, S., Agarwal, K., 2021. Mitochondrial metabolic manipulation by SARS-CoV-2 in peripheral blood mononuclear cells of patients with COVID-19. Am. J. Physiol. Cell Physiol. 320, C57–C65.

Albornoz, E.A., Amarilla, A.A., Modhiran, N., Parker, S., Li, X.X., Wijesundara, D.K., Aguado, J., Zamora, A.P., McMillan, C.L.D., Liang, B., 2022. SARS-CoV-2 drives NLRP3 inflammasome activation in human microglia through spike protein. Mol. Psychiatr. 1–16.

Antonini, A., Leta, V., Teo, J., Chaudhuri, K.R., 2020. Outcome of Parkinson's disease patients affected by COVID-19. Mov. Disord. 35, 905–908.

Barhoumi, T., Alghanem, B., Shaibah, H., Mansour, F.A., Alamri, H.S., Akiel, M.A., Alroqi, F., Boudjelal, M., 2021. SARS-CoV-2 coronavirus spike protein-induced apoptosis, inflammatory, and oxidative stress responses in THP-1-like-macrophages: potential role of angiotensin-converting enzyme inhibitor (perindopril). Front. Immunol. 12.

Bartolini, D., Stabile, A.M., Bastianelli, S., Giustarini, D., Pierucci, S., Busti, C., Vacca, C., Gidari, A., Francisci, D., Castronari, R., Mencacci, A., Di Cristina, M., Focaia, R., Sabbatini, S., Rende, M., Gioiello, A., Cruciani, G., Rossi, R., Galli, F., 2021. SARS-CoV2 infection impairs the metabolism and redox function of cellular glutathione. Redox Biol. 45, 102041.

Bertoldi, M., 2014. Mammalian Dopa decarboxylase: structure, catalytic activity and inhibition. Arch. Biochem. Biophys. 546, 1–7.

Bolte, S., Cordelières, F.P., 2006. A guided tour into subcellular colocalization analysis in light microscopy. J. Microsc. 224, 213–232.

Broderick, C., Calle, I.R., Carballa, A.G., Gómez-Rial, J., Li, H.K., Mehta, R., Jackson, H., Salas, A., Martinón-Torres, F., Sriskandan, S., Levin, M., Kaforou, M., Group, the, B. C., G, C.S., 2022. Pseudotemporal whole blood transcriptional profiling of COVID-19 patients stratified by clinical severity reveals differences in immune responses and possible role of monoamine oxidase B. Preprint at. https://doi.org/10.1101/2022.05.26.22274729.

Burke, W.J., Kumar, V.B., Pandey, N., Panneton, W.M., Gan, Q., Franko, M.W., O'Dell, M., Li, S.W., Pan, Y., Chung, H.D., 2008. Aggregation of α-synuclein by DOPAL, the monoamine oxidase metabolite of dopamine. Acta Neuropathol. 115, 193–203.

Butowt, R., Bilinska, K., 2020. SARS-CoV-2: olfaction, brain infection, and the urgent need for clinical samples allowing earlier virus detection. ACS Chem. Neurosci. 11, 1200–1203.

Caielli, S., Athale, S., Domic, B., Murat, E., Chandra, M., Banchereau, R., Baisch, J., Phelps, K., Clayton, S., Gong, M., 2016. Oxidized mitochondrial nucleoids released by neutrophils drive type I interferon production in human lupus. J. Exp. Med. 213, 697–713.

Cantuti-Castelvetri, L., Ojha, R., Pedro, L.D., Djannatian, M., Franz, J., Kuivanen, S., van der Meer, F., Kallio, K., Kaya, T., Anastasina, M., 2020. Neuropilin-1 facilitates SARS-CoV-2 cell entry and infectivity. Science 370, 856–860.

Chen, R., Wang, K., Yu, J., Howard, D., French, L., Chen, Z., Wen, C., Xu, Z., 2021. The spatial and cell-type distribution of SARS-CoV-2 receptor ACE2 in the human and mouse brains. Front. Neurol. 11, 1860.

Clough, E., Inigo, J., Chandra, D., Chaves, L., Reynolds, J.L., Aalinkeel, R., Schwartz, S. A., Khmaladze, A., Mahajan, S.D., 2021. Mitochondrial dynamics in SARS-COV2 spike protein treated human microglia: implications for neuro-COVID. J. Neuroimmune Pharmacol. 16, 770–784.

Codo, A.C., Davanzo, G.G., de Brito Monteiro, L., de Souza, G.F., Muraro, S.P., Virgilio-da-Silva, J.V., Prodonoff, J.S., Carregari, V.C., de Biagi Junior, C.A.O., Crunfli, F., 2020. Elevated glucose levels favor SARS-CoV-2 infection and monocyte response through a HIF-1α/glycolysis-dependent axis. Cell Metabol. 32, 437–446.

Cohen, M.E., Eichel, R., Steiner-Birmanns, B., Janah, A., Ioshpa, M., Bar-Shalom, R., Paul, J.J., Gaber, H., Skrahina, V., Bornstein, N.M., 2020. A case of probable Parkinson's disease after SARS-CoV-2 infection. Lancet Neurol. 19, 804–805.

Crunfli, F., Carregari, V.C., Veras, F.P., Silva, L.S., Nogueira, M.H., Antunes, A.S.L.M., Vendramini, P.H., Valença, A.G.F., Brandão-Teles, C., da Silva Zuccoli, G., Reis-De-Oliveira, G., Silva-Costa, L.C., Saia-Cereda, V.M., Smith, B.J., Codo, A.C., de Souza, G.F., Muraro, S.P., Parise, P.L., Toledo-Teixeira, D.A., de Castro, I.M.S., Melo, B.M., Almeida, G.M., Firmino, E.M.S., Paiva, I.M., Silva, B.M.S., Guimarães, R. M., Mendes, N.D., Ludwig, R.L., Ruiz, G.P., Knittel, T.L., Davanzo, G.G., Gerhardt, J. A., Rodrigues, P.B., Forato, J., Amorim, M.R., Brunetti, N.S., Martini, M.C., Benatti, M.N., Batah, S.S., Siyuan, L., João, R.B., Aventurato, I.K., de Brito, M.R., Mendes, M.J., da Costa, B.A., Alvim, M.K.M., da Silva Junior, J.R., Damião, L.L., de Sousa, I.M.P., da Rocha, E.D., Gonçalves, S.M., Lopes da Silva, L.H., Bettini, V., Campos, B.M., Ludwig, G., Tavares, L.A., Pontelli, M.C., Viana, R.M.M., Martins, R. B., Vieira, A.S., Alves-Filho, J.C., Arruda, E., Podolsky-Gondim, G.G., Santos, M.V., Neder, L., Damasio, A., Rehen, S., Vinolo, M.A.R., Munhoz, C.D., Louzada-Junior, P., Oliveira, R.D., Cunha, F.Q., Nakaya, H.I., Mauad, T., Duarte-Neto, A.N., da Silva, L.F. F., Dolhnikoff, M., Saldiva, P.H.N., Farias, A.S., Cendes, F., Moraes-Vieira, P.M.M., Fabro, A.T., Sebollela, A., Proença-Modena, J.L., Yasuda, C.L., Mori, M.A., Cunha, T. M., Martins-De-Souza, D., 2022. Morphological, cellular, and molecular basis of brain infection in COVID-19 patients. Proc. Natl. Acad. Sci. U.S.A. 119, e2200960119.

Cunha, B.A., 2004. Influenza: historical aspects of epidemics and pandemics. Infect. Dis. Clin. 18, 141–155.

Cuperlovic-Culf, M., Cunningham, E.L., Teimoorinia, H., Surendra, A., Pan, X., Bennett, S.A.L., Jung, M., McGuiness, B., Passmore, A.P., Beverland, D., 2021. Metabolomics and computational analysis of the role of monoamine oxidase activity in delirium and SARS-COV-2 infection. Sci. Rep. 11, 1–14.

de Oliveira, L.G., de Souza Angelo, Y., Yamamoto, P., Carregari, V.C., Crunfli, F., Reis-de-Oliveira, G., Costa, L., Vendramini, P.H., Duque, É.A., dos Santos, N.B., Firmino, E. M., Paiva, I.M., Almeida, G.M., Sebollela, A., Polonio, C.M., Zanluqui, N.G., de Oliveira, M.G., da Silva, P., Davanzo, G.G., Ayupe, M.C., Salgado, C.L., de Souza Filho, A.F., de Araújo, M.V., Silva-Pereira, T.T., de Almeida Campos, A.C., Góes, L.G. B., dos Passos Cunha, M., Caldini, E.G., D'Império Lima, M.R., Fonseca, D.M., de Sá Guimarães, A.M., Minoprio, P.C., Munhoz, C.D., Mori, C.M.C., Moraes-Vieira, P.M., Cunha, T.M., Martins-de-Souza, D., Peron, J.P.S., 2022. SARS-CoV-2 infection impacts carbon metabolism and depends on glutamine for replication in Syrian hamster astrocytes. J. Neurochem. 163, 113–132.

Dezsi, L., Vecsei, L., 2017. Monoamine oxidase B inhibitors in Parkinson's disease. CNS Neurol. Disord.: Drug Targets 16, 425–439.

Diwan, A., Koesters, A.G., Odley, A.M., Pushkaran, S., Baines, C.P., Spike, B.T., Daria, D., Jegga, A.G., Geiger, H., Aronow, B.J., 2007. Unrestrained erythroblast development in Nix−/− mice reveals a mechanism for apoptotic modulation of erythropoiesis. Proc. Natl. Acad. Sci. USA 104, 6794–6799.

Douaud, G., Lee, S., Alfaro-Almagro, F., Arthofer, C., Wang, C., McCarthy, P., Lange, F., Andersson, J.L.R., Griffanti, L., Duff, E., 2022. SARS-CoV-2 is associated with changes in brain structure in UK Biobank. Nature 604, 697–707.

Dringen, R., Hirrlinger, J., 2003. Glutathione pathways in the brain. Biol. Chem. 384, 505–516.

Faber, I., Brandão, P.R.P., Menegatti, F., de Carvalho Bispo, D.D., Maluf, F.B., Cardoso, F., 2020. Coronavirus disease 2019 and parkinsonism: a non-post-encephalitic case. Mov. Disord. 35, 1721–1722.

Fernández-Castañeda, A., Lu, P., Geraghty, A.C., Song, E., Lee, M.-H., Wood, J., O'Dea, M.R., Dutton, S., Shamardani, K., Nwangwu, K., 2022. Mild respiratory COVID can cause multi-lineage neural cell and myelin dysregulation. Cell 185, 2452–2468.

Flynn, R.A., Belk, J.A., Qi, Y., Yasumoto, Y., Wei, J., Alfajaro, M.M., Shi, Q., Mumbach, M.R., Limaye, A., DeWeirdt, P.C., 2021. Discovery and functional interrogation of SARS-CoV-2 RNA-host protein interactions. Cell 184, 2394–2411.

Frühbeck, G., Catalán, V., Valentí, V., Moncada, R., Gómez-Ambrosi, J., Becerril, S., Silva, C., Portincasa, P., Escalada, J., Rodríguez, A., 2021. FNDC4 and FNDC5 reduce SARS-CoV-2 entry points and spike glycoprotein S1-induced pyroptosis, apoptosis, and necroptosis in human adipocytes. Cell. Mol. Immunol. 18, 2457–2459.

Gibellini, L., De Biasi, S., Paolini, A., Borella, R., Boraldi, F., Mattioli, M., Lo Tartaro, D., Fidanza, L., Caro-Maldonado, A., Meschiari, M., 2020. Altered bioenergetics and mitochondrial dysfunction of monocytes in patients with COVID-19 pneumonia. EMBO Mol. Med. 12, e13001.

Green, D.R., Kroemer, G., 2004. The pathophysiology of mitochondrial cell death. Science 305, 626–629.

Guedj, E., Million, M., Dudouet, P., Tissot-Dupont, H., Bregeon, F., Cammilleri, S., Raoult, D., 2021. 18F-FDG brain PET hypometabolism in post-SARS-CoV-2 infection: substrate for persistent/delayed disorders? Eur. J. Nucl. Med. Mol. Imag. 48, 592–595.

Gullberg, M., Andersson, A.-C., 2010. Visualization and quantification of protein-protein interactions in cells and tissues. Nat. Methods 7, v–vi.

Guo, W., Jiang, L., Bhasin, S., Khan, S.M., Swerdlow, R.H., 2009. DNA extraction procedures meaningfully influence qPCR-based mtDNA copy number determination. Mitochondrion 9, 261–265.

Hanna, R.A., Quinsay, M.N., Orogo, A.M., Giang, K., Rikka, S., Gustafsson, A.B., 2012. Microtubule-associated protein 1 light chain 3 (LC3) interacts with Bnip3 protein to selectively remove endoplasmic reticulum and mitochondria via autophagy. J. Biol. Chem. 287, 19094–19104.

Harrington, J.S., Huh, J.-W., Schenck, E.J., Nakahira, K., Siempos, I.I., Choi, A.M.K., 2019. Circulating mitochondrial DNA as predictor of mortality in critically ill patients: a systematic review of clinical studies. Chest 156, 1120–1136.

Harrison, S.C., 2015. Viral membrane fusion. Virology 479, 498–507.

Heikkila, R.E., Manzino, L., Cabbat, F.S., Duvoisin, R.C., 1984. Protection against the dopaminergic neurotoxicity of 1-methyl-4-phenyl-1, 2, 5, 6-tetrahydropyridine by monoamine oxidase inhibitors. Nature 311, 467–469.

Helms, J., Kremer, S., Merdji, H., Clere-Jehl, R., Schenck, M., Kummerlen, C., Collange, O., Boulay, C., Fafi-Kremer, S., Ohana, M., 2020. Neurologic features in severe SARS-CoV-2 infection. N. Engl. J. Med. 382, 2268–2270.

Hirrlinger, J., König, J., Keppler, D., Lindenau, J., Schulz, J.B., Dringen, R., 2001. The multidrug resistance protein MRP1 mediates the release of glutathione disulfide from rat astrocytes during oxidative stress. J. Neurochem. 76, 627–636.

Hoffmann, M., Kleine-Weber, H., Schroeder, S., Krüger, N., Herrler, T., Erichsen, S., Schiergens, T.S., Herrler, G., Wu, N.-H., Nitsche, A., 2020. SARS-CoV-2 cell entry depends on ACE2 and TMPRSS2 and is blocked by a clinically proven protease inhibitor. Cell 181, 271–280.

Hok, L., Rimac, H., Mavri, J., Vianello, R., 2022. COVID-19 infection and neurodegeneration: computational evidence for interactions between the SARS-CoV-2 spike protein and monoamine oxidase enzymes. Comput. Struct. Biotechnol. J. 20, 1254–1263.

Hosp, J.A., Dressing, A., Blazhenets, G., Bormann, T., Rau, A., Schwabenland, M., Thurow, J., Wagner, D., Waller, C., Niesen, W.D., 2021. Cognitive impairment and altered cerebral glucose metabolism in the subacute stage of COVID-19. Brain 144, 1263–1276.

Ito, K., Eguchi, Y., Imagawa, Y., Akai, S., Mochizuki, H., Tsujimoto, Y., 2017. MPP+ induces necrostatin-1- and ferrostatin-1-sensitive necrotic death of neuronal SH-SY5Y cells. Cell Death Dis. 3, 1–10.

Javitch, J.A., D'Amato, R.J., Strittmatter, S.M., Snyder, S.H., 1985. Parkinsonism-inducing neurotoxin, N-methyl-4-phenyl-1, 2, 3, 6-tetrahydropyridine: uptake of the metabolite N-methyl-4-phenylpyridine by dopamine neurons explains selective toxicity. Proc. Natl. Acad. Sci. U.S.A. 82, 2173–2177.

Jiang, H., Jiang, Q., Liu, W., Feng, J., 2006. Parkin suppresses the expression of monoamine oxidases. J. Biol. Chem. 281, 8591–8599.
Jiang, T., Sun, Q., Chen, S., 2016. Oxidative stress: a major pathogenesis and potential therapeutic target of antioxidative agents in Parkinson's disease and Alzheimer's disease. Prog. Neurobiol. 147, 1–19.
Kaludercic, N., Carpi, A., Nagayama, T., Sivakumaran, V., Zhu, G., Lai, E.W., Bedja, D., De Mario, A., Chen, K., Gabrielson, K.L., 2014. Monoamine oxidase B prompts mitochondrial and cardiac dysfunction in pressure overloaded hearts. Antioxidants Redox Signal. 20, 267–280.
Kamerkar, S.C., Kraus, F., Sharpe, A.J., Pucadyil, T.J., Ryan, M.T., 2018. Dynamin-related protein 1 has membrane constricting and severing abilities sufficient for mitochondrial and peroxisomal fission. Nat. Commun. 9, 1–15.
Kane, D.J., Ord, T., Anton, R., Bredesen, D.E., 1995. Expression of bcl-2 inhibits necrotic neural cell death. J. Neurosci. Res. 40, 269–275.
Kantonen, J., Mahzabin, S., Mäyränpää, M.I., Tynninen, O., Paetau, A., Andersson, N., Sajantila, A., Vapalahti, O., Carpén, O., Kekäläinen, E., 2020. Neuropathologic features of four autopsied COVID-19 patients. Brain Pathol. 30, 1012.
Kim, J.-Y., Cho, J.-J., Ha, J., Park, J.-H., 2002. The carboxy terminal C-tail of BNip3 is crucial in induction of mitochondrial permeability transition in isolated mitochondria. Arch. Biochem. Biophys. 398, 147–152.
Kim, I., Rodriguez-Enriquez, S., Lemasters, J.J., 2007. Selective degradation of mitochondria by mitophagy. Arch. Biochem. Biophys. 462, 245–253.
Kim, E.S., Jeon, M.-T., Kim, K.-S., Lee, S., Kim, S., Kim, D.-G., 2021. Spike proteins of SARS-CoV-2 induce pathological changes in molecular delivery and metabolic function in the brain endothelial cells. Viruses 13, 2021.
Krasemann, S., Haferkamp, U., Pfefferle, S., Woo, M.S., Heinrich, F., Schweizer, M., Appelt-Menzel, A., Cubukova, A., Barenberg, J., Leu, J., 2022. The blood-brain barrier is dysregulated in COVID-19 and serves as a CNS entry route for SARS-CoV-2. Stem Cell Rep. 17, 307–320.
Kubasiak, L.A., Hernandez, O.M., Bishopric, N.H., Webster, K.A., 2002. Hypoxia and acidosis activate cardiac myocyte death through the Bcl-2 family protein BNIP3. Proc. Natl. Acad. Sci. U.S.A. 99, 12825–12830.
Kubli, D.A., Ycaza, J.E., Gustafsson, Å.B., 2007. Bnip3 mediates mitochondrial dysfunction and cell death through Bax and Bak. Biochem. J. 405, 407–415.
Kumar, P., Osahon, O., Vides, D.B., Hanania, N., Minard, C.G., Sekhar, R.V., 2021. Severe glutathione deficiency, oxidative stress and oxidant damage in adults hospitalized with COVID-19: implications for GlyNAC (Glycine and N-Acetylcysteine) supplementation. Antioxidants 11, 50.
Lage, S.L., Amaral, E.P., Hilligan, K.L., Laidlaw, E., Rupert, A., Namasivayan, S., Rocco, J., Galindo, F., Kellogg, A., Kumar, P., 2021. Persistent oxidative stress and inflammasome activation in CD14highCD16− monocytes from COVID-19 patients. Front. Immunol. 12, 799558.
Lei, Y., Zhang, J., Schiavon, C.R., He, M., Chen, L., Shen, H., Zhang, Y., Yin, Q., Cho, Y., Andrade, L., 2021. SARS-CoV-2 spike protein impairs endothelial function via downregulation of ACE 2. Circ. Res. 128, 1323–1326.
Li, F., Li, J., Wang, P.-H., Yang, N., Huang, J., Ou, J., Xu, T., Zhao, X., Liu, T., Huang, X., 2021. SARS-CoV-2 spike promotes inflammation and apoptosis through autophagy by ROS-suppressed PI3K/AKT/mTOR signaling. Biochim. Biophys. Acta, Mol. Basis Dis. 1867, 166260.
Liaghati, A., Pileggi, C.A., Parmar, G., Patten, D.A., Hadzimustafic, N., Cuillerier, A., Menzies, K.J., Burelle, Y., Harper, M.-E., 2021. Grx2 regulates skeletal muscle mitochondrial structure and autophagy. Front. Physiol. 12, 604210.
Mallajosyula, J.K., Kaur, D., Chinta, S.J., Rajagopalan, S., Rane, A., Nicholls, D.G., Di Monte, D.A., Macarthur, H., Andersen, J.K., 2008. MAO-B elevation in mouse brain astrocytes results in Parkinson's pathology. PLoS One 3, e1616.
Manca, R., De Marco, M., Ince, P.G., Venneri, A., 2021. Heterogeneity in regional damage detected by neuroimaging and neuropathological studies in older adults with COVID-19: a cognitive-neuroscience systematic review to inform the long-term impact of the virus on neurocognitive trajectories. Front. Aging Neurosci. 13, 646908.
Manne, B.K., Denorme, F., Middleton, E.A., Portier, I., Rowley, J.W., Stubben, C., Petrey, A.C., Tolley, N.D., Guo, L., Cody, M., 2020. Platelet gene expression and function in patients with COVID-19. Blood 136, 1317–1329.
Mao, L., Jin, H., Wang, M., Hu, Y., Chen, S., He, Q., Chang, J., Hong, C., Zhou, Y., Wang, D., 2020. Neurologic manifestations of hospitalized patients with coronavirus disease 2019 in Wuhan, China. JAMA Neurol. 77, 683–690.
Matschke, J., Lütgehetmann, M., Hagel, C., Sperhake, J.P., Schröder, A.S., Edler, C., Mushumba, H., Fitzek, A., Allweiss, L., Dandri, M., 2020. Neuropathology of patients with COVID-19 in Germany: a post-mortem case series. Lancet Neurol. 19, 919–929.
Miller, B., Silverstein, A., Flores, M., Cao, K., Kumagai, H., Mehta, H.H., Yen, K., Kim, S.-J., Cohen, P., 2021. Host mitochondrial transcriptome response to SARS-CoV-2 in multiple cell models and clinical samples. Sci. Rep. 11, 1–10.
Mitochondrial metabolic manipulation by SARS-CoV-2 in peripheral blood mononuclear cells of patients with COVID-19. Am. J. Physiol. Cell Physiol. 320, C57-C65.
Moriguchi, S., Wilson, A.A., Miler, L., Rusjan, P.M., Vasdev, N., Kish, S.J., Rajkowska, G., Wang, J., Bagby, M., Mizrahi, R., 2019. Monoamine oxidase B total distribution volume in the prefrontal cortex of major depressive disorder: an [11C] SL25. 1188 positron emission tomography study. JAMA Psychiatr. 76, 634–641.
Mpekoulis, G., Frakolaki, E., Taka, S., Ioannidis, A., Vassiliou, A.G., Kalliampakou, K.I., Patas, K., Karakasiliotis, I., Aidinis, V., Chatzipanagiotou, S., 2021. Alteration of L-Dopa decarboxylase expression in SARS-CoV-2 infection and its association with the interferon-inducible ACE2 isoform. PLoS One 16, e0253458.
Mukerji, S.S., Solomon, I.H., 2021. What can we learn from brain autopsies in COVID-19? Neurosci. Lett. 742, 135528.
Nagatsu, T., Sawada, M., 2006. Molecular mechanism of the relation of monoamine oxidase B and its inhibitors to Parkinson's disease: possible implications of glial cells. J. Neural. Transm. Suppl. 53–65.
Nicotra, A., Parvez, S.H., 2000. Cell death induced by MPTP, a substrate for monoamine oxidase B. Toxicology 153, 157–166.
Obata, Y., Kubota-Sakashita, M., Kasahara, T., Mizuno, M., Nemoto, T., Kato, T., 2022. Phenethylamine is a substrate of monoamine oxidase B in the paraventricular thalamic nucleus. Sci. Rep. 12, 1–11.
Oldfield, V., Keating, G.M., Perry, C.M., 2007. Rasagiline: a review of its use in the management of Parkinson's disease. Drugs 67 (12), 1725–1747.
Ou, X., Liu, Y., Lei, X., Li, P., Mi, D., Ren, L., Guo, L., Guo, R., Chen, T., Hu, J., 2020. Characterization of spike glycoprotein of SARS-CoV-2 on virus entry and its immune cross-reactivity with SARS-CoV. Nat. Commun. 11, 1–12.
Pellegrini, L., Albecka, A., Mallery, D.L., Kellner, M.J., Paul, D., Carter, A.P., James, L.C., Lancaster, M.A., 2020. SARS-CoV-2 infects the brain choroid plexus and disrupts the blood-CSF barrier in human brain organoids. Cell Stem Cell 27, 951–961.
Peluso, M.J., Deeks, S.G., Mustapic, M., Kapogiannis, D., Henrich, T.J., Lu, S., Goldberg, S.A., Hoh, R., Chen, J.Y., Martinez, E.O., 2022. SARS-CoV-2 and mitochondrial proteins in neural-derived Exosomes of COVID-19. Ann Neurol. 91, 772–781.
Pileggi, C.A., Hedges, C.P., Segovia, S.A., Markworth, J.F., Durainayagam, B.R., Gray, C., Zhang, X.D., Barnett, M.P.G., Vickers, M.H., Hickey, A.J., Reynolds, C.M., Cameron-Smith, D., 2016. Maternal fat Diet alters skeletal muscle mitochondrial catalytic activity in adult Male rat offspring. Front. Physiol. 7, 546.
Pizzinat, N., Copin, N., Vindis, C., Parini, A., Cambon, C., 1999. Reactive oxygen species production by monoamine oxidases in intact cells. Naunyn-Schmiedeberg's Arch. Pharmacol. 359, 428–431.
Poletti, S., Paolini, M., Mazza, M.G., Palladini, M., Furlan, R., Querini, P.R., Benedetti, F., Group, C.B.O.C.S., 2022. Lower levels of glutathione in the anterior cingulate cortex associate with depressive symptoms and white matter hyperintensities in COVID-19 survivors. Eur. Neuropsychopharmacol 61, 71–77.
Polonikov, A., 2020. Endogenous deficiency of glutathione as the most likely cause of serious manifestations and death in COVID-19 patients. ACS Infect. Dis. 6, 1558–1562.
Ramachandran, K., Maity, S., Muthukumar, A.R., Kandala, S., Tomar, D., Abd El-Aziz, T. M., Allen, C., Sun, Y., Venkatesan, M., Madaris, T.R., 2022. SARS-CoV-2 infection enhances mitochondrial PTP complex activity to perturb cardiac energetics. iScience 25, 103722.
Raman, B., Cassar, M.P., Tunnicliffe, E.M., Filippini, N., Griffanti, L., Alfaro-Almagro, F., Okell, T., Sheerin, F., Xie, C., Mahmod, M., 2021. Medium-term effects of SARS-CoV-2 infection on multiple vital organs, exercise capacity, cognition, quality of life and mental health, post-hospital discharge. EClinicalMedicine 31, 100683.
Ramsay, R.R., Singer, T.P., 1986. Energy-dependent uptake of N-methyl-4-phenylpyridinium, the neurotoxic metabolite of 1-methyl-4-phenyl-1, 2, 3, 6-tetrahydropyridine, by mitochondria. J. Biol. Chem. 261, 7585–7587.
Rhea, E.M., Logsdon, A.F., Hansen, K.M., Williams, L.M., Reed, M.J., Baumann, K.K., Holden, S.J., Raber, J., Banks, W.A., Erickson, M.A., 2021. The S1 protein of SARS-CoV-2 crosses the blood–brain barrier in mice. Nat. Neurosci. 24, 368–378.
Richard, V.R., Gaither, C., Popp, R., Chaplygina, D., Brzhozovskiy, A., Kononikhin, A., Mohammed, Y., Zahedi, R.P., Nikolaev, E.N., Borchers, C.H., 2022. Early prediction of COVID-19 patient survival by targeted plasma multi-omics and machine learning. Mol. Cell. Proteomics 21, 100277.
Romão, P.R.T., Teixeira, P.C., Schipper, L., da Silva, I., Santana Filho, P., Júnior, L.C.R., Peres, A., da Fonseca, S.G., Monteiro, M.C., Lira, F.S., 2022. Viral load is associated with mitochondrial dysfunction and altered monocyte phenotype in acute severe SARS-CoV-2 infection. Int. Immunopharm. 108, 108697.
Saito, K., Ishikawa, R., Kitamura, I., Ogawa, K., Arakawa, N., Sun, Y., Imai, K., Maeda, T., Saito, Y., Hasegawa, C., 2022. Characterization of serotonin as a candidate biomarker of severity and prognosis of COVID-19 using LC/MS analysis. J. Pharmacol. Sci. 150, 49–55.
Shang, J., Wan, Y., Luo, C., Ye, G., Geng, Q., Auerbach, A., Li, F., 2020a. Cell entry mechanisms of SARS-CoV-2. Proc. Natl. Acad. Sci. U.S.A. 117, 11727–11734.
Shang, J., Ye, G., Shi, K., Wan, Y., Luo, C., Aihara, H., Geng, Q., Auerbach, A., Li, F., 2020b. Structural basis of receptor recognition by SARS-CoV-2. Nature 581, 221–224.
Shang, C., Liu, Z., Zhu, Y., Lu, J., Ge, C., Zhang, C., Li, N., Jin, N., Li, Y., Tian, M., 2021. SARS-CoV-2 causes mitochondrial dysfunction and mitophagy impairment. Front. Microbiol. 12, 780768.
Shen, B., Yi, X., Sun, Y., Bi, X., Du, J., Zhang, C., Quan, S., Zhang, F., Sun, R., Qian, L., Ge, W., Liu, W., Liang, S., Chen, Hao, Zhang, Y., Li, J., Xu, J., He, Z., Chen, B., Wang, J., Yan, H., Zheng, Y., Wang, D., Zhu, J., Kong, Z., Kang, Z., Liang, X., Ding, X., Ruan, G., Xiang, N., Cai, X., Gao, H., Li, L., Li, S., Xiao, Q., Lu, T., Zhu, Y., Liu, H., Chen, Haixiao, Guo, T., 2020. Proteomic and metabolomic characterization of COVID-19 patient sera. Cell 182, 59–72.e15.
Shirato, K., Kizaki, T., 2021. SARS-CoV-2 spike protein S1 subunit induces pro-inflammatory responses via toll-like receptor 4 signaling in murine and human macrophages. Heliyon 7, e06187.
Singh, N., Singh, A.B., 2020. S2 subunit of SARS-nCoV-2 interacts with tumor suppressor protein p53 and BRCA: an in silico study. Transl Oncol 13, 100814.
Smeyne, R.J., Eells, J.B., Chatterjee, D., Byrne, M., Akula, S.M., Sriramula, S., O'Rourke, D.P., Schmidt, P., 2022. COVID-19 infection enhances susceptibility to oxidative-stress induced parkinsonism. Mov. Disord. 37, 1394–1404.
Smirnova, E., Griparic, L., Shurland, D.-L., Van Der Bliek, A.M., 2001. Dynamin-related protein Drp1 is required for mitochondrial division in mammalian cells. Mol. Biol. Cell 12, 2245–2256.

Smith, A.K., White, P.D., Aslakson, E., Vollmer-Conna, U., Rajeevan, M.S., 2006. Polymorphisms in genes regulating the HPA axis associated with empirically delineated classes of unexplained chronic fatigue. Pharmacogenomics 7, 387–394.
Solis, O., Beccari, A.R., Iaconis, D., Talarico, C., Ruiz-Bedoya, C.A., Nwachukwu, J.C., Cimini, A., Castelli, V., Bertini, R., Montopoli, M., Cocetta, V., Borocci, S., Prandi, I. G., Flavahan, K., Bahr, M., Napiorkowski, A., Chillemi, G., Ooka, M., Yang, X., Zhang, S., Xia, M., Zheng, W., Bonaventura, J., Pomper, M.G., Hooper, J.E., Morales, M., Rosenberg, A.Z., Nettles, K.W., Jain, S.K., Allegretti, M., Michaelides, M., 2022. The SARS-CoV-2 spike protein binds and modulates estrogen receptors. Sci. Adv. 8, 4150.
Song, E., Zhang, C., Israelow, B., Lu-Culligan, A., Prado, A.V., Skriabine, S., Lu, P., Weizman, O.-E., Liu, F., Dai, Y., 2021. Neuroinvasion of SARS-CoV-2 in human and mouse brain. J. Exp. Med. 218, e20202135.
Spinazzi, M., Casarin, A., Pertegato, V., Salviati, L., Angelini, C., 2012. Assessment of mitochondrial respiratory chain enzymatic activities on tissues and cultured cells. Nat. Protoc. 7, 1235–1246.
Stefano, G.B., Ptacek, R., Ptackova, H., Martin, A., Kream, R.M., 2021. Selective neuronal mitochondrial targeting in SARS-CoV-2 infection affects cognitive processes to induce 'brain fog'and results in behavioral changes that favor viral survival. Med. Sci. Mon. Int. Med. J. Exp. Clin. Res. 27, e930886-1.
Stein, S.R., Ramelli, S.C., Grazioli, A., Chung, J.Y., Singh, M., Yinda, C.K., Winkler, C.W., Sun, J., Dickey, J.M., Ylaya, K., Ko, S.H., Platt, A.P., Burbelo, P.D., Quezado, M., Pittaluga, S., Purcell, M., Munster, V.J., Belinky, F., Ramos-Benitez, M.J., Boritz, E. A., Lach, I.A., Herr, D.L., Rabin, J., Saharia, K.K., Madathil, R.J., Tabatabai, A., Soherwardi, S., McCurdy, M.T., Babyak, A.L., Perez Valencia, L.J., Curran, S.J., Richert, M.E., Young, W.J., Young, S.P., Gasmi, B., Sampaio De Melo, M., Desar, S., Tadros, S., Nasir, N., Jin, X., Rajan, S., Dikoglu, E., Ozkaya, N., Smith, G., Emanuel, E.R., Kelsall, B.L., Olivera, J.A., Blawas, M., Star, R.A., Hays, N., Singireddy, S., Wu, J., Raja, K., Curto, R., Chung, J.E., Borth, A.J., Bowers, K.A., Weichold, A.M., Minor, P.A., Moshref, M.A.N., Kelly, E.E., Sajadi, M.M., Scalea, T. M., Tran, D., Dahi, S., Deatrick, K.B., Krause, E.M., Herrold, J.A., Hochberg, E.S., Cornachione, C.R., Levine, A.R., Richards, J.E., Elder, J., Burke, A.P., Mazzeffi, M.A., Christenson, R.H., Chancer, Z.A., Abdulmahdi, M., Sopha, S., Goldberg, T., Sangwan, Y., Sudano, K., Blume, D., Radin, B., Arnouk, M., Eagan, J.W., Palermo, R., Harris, A.D., Pohida, T., Garmendia-Cedillos, M., Dold, G., Saglio, E., Pham, P., Peterson, K.E., Cohen, J.I., de Wit, E., Vannella, K.M., Hewitt, S.M., Kleiner, D.E., Chertow, D.S., 2022. SARS-CoV-2 infection and persistence in the human body and brain at autopsy. Nature 612, 758–763.
Suzuki, Y.J., Nikolaienko, S.I., Dibrova, V.A., Dibrova, Y.V., Vasylyk, V.M., Novikov, M. Y., Shults, N.V., Gychka, S.G., 2021. SARS-CoV-2 spike protein-mediated cell signaling in lung vascular cells. Vasc. Pharmacol. 137, 106823.
Swank, Z., Senussi, Y., Manickas-Hill, Z., Yu, X.G., Li, J.Z., Alter, G., Walt, D.R., 2023. Persistent circulating severe acute respiratory syndrome coronavirus 2 spike is associated with post-acute coronavirus disease 2019 sequelae. Clin. Infect. Dis. 76 (3), e487–e490.
Taquet, M., Geddes, J.R., Husain, M., Luciano, S., Harrison, P.J., 2021. 6-month neurological and psychiatric outcomes in 236 379 survivors of COVID-19: a retrospective cohort study using electronic health records. Lancet Psychiatr. 8, 416–427.
Tipton, K.F., 2018. 90 years of monoamine oxidase: some progress and some confusion. J. Neural. Transm. 125, 1519–1551.
Tipton, K.F., Davey, G., Motherway, M., 2000. Monoamine oxidase assays. Curr. Protoc. Pharmacol. 9, 3–6.
Tischner, D., Manzl, C., Soratroi, C., Villunger, A., Krumschnabel, G., 2012. Necrosis-like death can engage multiple pro-apoptotic Bcl-2 protein family members. Apoptosis 17, 1197–1209.
Turrens, J., 1997. Superoxide production by the mitochondrial respiratory chain. Biosci. Rep. 17, 3–8.
Twig, G., Elorza, A., Molina, A.J., Mohamed, H., Wikstrom, J.D., Walzer, G., Stiles, L., Haigh, S.E., Katz, S., Las, G., Alroy, J., Wu, M., Py, B.F., Yuan, J., Deeney, J.T., Corkey, B.E., Shirihai, O.S., 2008. Fission and selective fusion govern mitochondrial segregation and elimination by autophagy. EMBO J. 27, 433–446.
Velde, C. Vande, Cizeau, J., Dubik, D., Alimonti, J., Brown, T., Israels, S., Hakem, R., Greenberg, A.H., 2000. BNIP3 and genetic control of necrosis-like cell death through the mitochondrial permeability transition pore. Mol. Cell Biol. 20, 5454–5468.
Wang, S., Quan, L., Chavarro, J.E., Slopen, N., Kubzansky, L.D., Koenen, K.C., Kang, J.H., Weisskopf, M.G., Branch-Elliman, W., Roberts, A.L., 2022. Associations of depression, anxiety, worry, perceived stress, and loneliness prior to infection with risk of post–COVID-19 conditions. JAMA Psychiatr. 79, 1081–1091.
Wei, Q., Yeung, M., Jurma, O.P., Andersen, J.K., 1996. Genetic elevation of monoamine oxidase levels in dopaminergic PC12 cells results in increased free radical damage and sensitivity to MPTP. J. Neurosci. Res. 46, 666–673.
Wu, K.E., Fazal, F.M., Parker, K.R., Zou, J., Chang, H.Y., 2020. RNA-GPS predicts SARS-CoV-2 RNA residency to host mitochondria and nucleolus. Cell Syst 11, 102–108.
Yang, L., Han, Y., Nilsson-Payant, B.E., Gupta, V., Wang, P., Duan, X., Tang, X., Zhu, J., Zhao, Z., Jaffré, F., 2020. A human pluripotent stem cell-based platform to study SARS-CoV-2 tropism and model virus infection in human cells and organoids. Cell Stem Cell 27, 125–136.
Youle, R.J., Narendra, D.P., 2011. Mechanisms of mitophagy. Nat. Rev. Mol. Cell Biol. 12, 9–14.
Yuan, L., Chen, Z., Song, S., Wang, S., Tian, C., Xing, G., Chen, X., Xiao, Z.-X., He, F., Zhang, L., 2015. p53 degradation by a coronavirus papain-like protease suppresses type I interferon signaling. J. Biol. Chem. 290, 3172–3182.
Zhang, C., Lin, M., Wu, R., Wang, X., Yang, B., Levine, A.J., Hu, W., Feng, Z., 2011. Parkin, a p53 target gene, mediates the role of p53 in glucose metabolism and the Warburg effect. N. Engl. J. Med. 108, 16259–16264.
Zhu, N., Zhang, D., Wang, W., Li, X., Yang, B., Song, J., Zhao, X., Huang, B., Shi, W., Lu, R., 2020. A novel coronavirus from patients with pneumonia in China, 2019. N. Engl. J. Med. 382, 727–733.